NASA TECHNICAL MEMORANDUM 104064

ENVIRONMENTAL FATIGUE OF AN Al-Li-Cu ALLOY: PART I - INTRINSIC CRACK PROPAGATION KINETICS IN HYDROGENOUS ENVIRONMENTS

Robert S. Piascik and Richard P. Gangloff

MARCH 1991

NASA

National Aeronautics and
Space Administration

Langley Research Center
Hampton, Virginia 23665

SUMMARY

Deleterious environmental effects on steady-state, intrinsic fatigue crack propagation (FCP) rates (da/dN) in peak aged Al-Li-Cu alloy 2090 are established by electrical potential monitoring of short cracks with programmed constant ΔK and K_{max} loading. Da/dN are equally unaffected by vacuum, purified helium and oxygen; but are accelerated in order of decreasing effectiveness by aqueous 1% NaCl with anodic polarization, pure water vapor, moist air and NaCl with cathodic polarization. While da/dN depends on $\Delta K^{4.0}$ for the inert gases, water vapor and chloride induce multiple power-laws and a transition growth rate "plateau". Environmental effects are strongest at low ΔK. Crack tip damage is ascribed to hydrogen embrittlement because of: accelerated da/dN due to part-per-million levels of H_2O without condensation, impeded molecular flow model predictions of the measured water vapor pressure dependence of da/dN as affected by mean crack opening, the lack of an effect of film-forming O_2, the likelihood for crack tip hydrogen production in NaCl, and the environmental and ΔK-process zone volume dependencies of the fatigue cracking modes. For NaCl, growth rates decrease with decreasing loading frequency, with the addition of passivating Li_2CO_3 and upon cathodic polarization. These variables increase crack surface film stability to reduce hydrogen absorption. Small crack effects are not observed for 2090, including the lack of: rapid growth and boundary arrest of a small crack in a single grain, and rapid growth of short cracks in NaCl. The environmental FCP resistance of 2090 is similar to other 2000 series alloys and is better than 7075.

I. INTRODUCTION

Precipitation hardened Al-Li-Cu based alloys are of considerable interest for aerospace applications because of low density, high stiffness, superior fatigue crack growth resistance and high cryogenic toughness[1-5]. Research has concentrated on improving those properties controlled by high angle grain boundaries, including low short transverse fracture toughness[6-9], localized aqueous corrosion[10-13] and intergranular stress corrosion cracking[14-16]. In contrast studies are lacking regarding environmental effects on fatigue crack growth and associated damage mechanisms.

The outstanding fatigue crack propagation (FCP) resistance of Al-Li alloys in moist air is controlled by two factors; increased extrinsic shielding by crack closure and reduced environmental embrittlement compared to other high strength aluminum alloys[17,18]. Increased elastic modulus may provide some improvement in cracking resistance. The strong effect of closure on FCP is traceable to the highly localized planar and reversible character of slip in under to peak aged Al-Li microstructures hardened by ordered coherent precipitates[19-21]. Such deformation exacerbates roughness induced closure by producing microscopic crack deflections, highly faceted fatigue crack surfaces and mode II displacements. The mechanical and microstructural factors which affect crack closure in Al-Li alloys are reviewed elsewhere[18].

Aluminum alloys are prone to cracking in water vapor or halogen bearing electrolytes and under monotonic or cyclic loading[22,23]. Extensive environmental FCP rate (da/dN) studies have been conducted on conventional 2000 and 7000 series aluminum alloys[23]. This work identified the effects of important variables including: stress intensity range ($\Delta K = K_{max} - K_{min}$)[24], stress ratio ($R = K_{min}/K_{max}$)[25,26], water vapor pressure[27-29], oxygen partial pressure[30], electrode potential[31-33], loading frequency[26-28,32,34], alloy composition[35], and deformation mode[36]. The preeminent mechanisms for environmental cracking of aluminum alloys include: hydrogen environment embrittlement[27,32,37-40], passive film formation/rupture/anodic dissolution[41] and surface film effects on plastic deformation[31,42].

Uncertainties exist regarding environmental fatigue in aluminum alloys. While hydrogen embrittlement is established for 2000 and 7000 series alloys in water vapor, cracking mechanisms for aqueous solutions are controversial because of the simultaneous action of hydrogen

2

production, metal dissolution and surface film formation[27,37]. Quantitative models for da/dN-ΔK were developed for specific chemical processes, but do not adequately describe interactive chemical and mechanical crack tip damage[23,40]. Environmental effects on near-threshold (ΔK_{th}) crack propagation[2] have not been extensively studied, despite the effort on mechanical fatigue threshold concepts[43]. Crack closure-environment and small crack-environment interactions have not been examined for aluminum alloys[29,44].

Understanding of environmental FCP in Al-Li based alloys is further limited compared to 2000 and 7000 series alloys. High angle grain boundary cracking of unrecrystallized Al-Li alloys in aqueous chloride under monotonic loading is understood[22,45,46], but is only relevant to environmental fatigue above the stress corrosion cracking threshold stress intensity (K_{ISCC}). Limited crack growth rate data have been reported for transgranular cycle-time-dependent environmental fatigue in Al-Li-Cu alloys. Studies demonstrated reductions in crack closure, and associated increases in da/dN, for Al-Li-Cu-Zr alloys in aqueous NaCl when compared to moist air or vacuum[47-50]. Hydrogen embrittlement was proposed as a fatigue damage mechanism[49,50], but this conclusion was not substantiated by data on the effects of variables which could implicate the cracking mechanism, by determinations of microscopic fatigue crack paths, and by modeling of crack tip damage.

While important to environmental fatigue in Al-Li-Cu based alloys, extrinsic shielding by crack closure complicates mechanistic interpretations of growth rate data. Closure has been either ignored, or da/dN data have been correlated with an effective stress intensity range ($\Delta K_{eff} = K_{max} - K_{closure}$), where $K_{closure}$ is measured using remote techniques. This approach may not sufficiently describe the mechanical crack tip driving force, particularly for near threshold da/dN[18,51]. An experimental method based on decreasing ΔK and increasing R at constant K_{max} provides an attractive alternative to minimize crack closure effects[26,52]. It is also important to guarantee that environmental crack growth rate data are steady state, or constant with varying crack size and exposure time at constant ΔK. Crack geometry can influence occluded crack chemistry and thus environmental crack growth rates[23,44,53]. This effect has not been considered for aluminum alloys. The experimental approach is designed based on these considerations.

---

[2]Near-threshold is defined as fatigue crack propagation at rates below 10^{-6} mm/cycle.

II. OBJECTIVE and APPROACH

The objective of this research is to characterize environmental effects on intrinsic FCP kinetics for an Al-Li-Cu alloy and to establish crack tip damage mechanisms independent of crack closure[54]3. This information is required for development of cracking resistant alloys and to enable long term, damage tolerant applications of aluminum alloys in aggressive environments.

The emphasis is on corrosion fatigue below K_{ISCC} and not affected by high angle grain boundaries. Crack growth rates are determined by direct current electrical potential monitoring of short fatigue cracks, coupled with programmed constant ΔK growth segments at constant K_{max} and various levels of R. This experimental method is used to: (a) minimize crack closure by short crack wake and high R, (b) study physically small fatigue cracks within single or multiple grains and in aqueous environments, (c) characterize chemical effects on da/dN at constant ΔK, and (d) measure near-ΔK_{th} fatigue at slow loading frequencies with small growth increments.

Moist air, water vapor, oxygen, vacuum, helium and aqueous chloride environments are employed. Gas pressure, electrode potential, ionic additions, loading frequency, and crack orientation are systematically varied to probe the contributions of hydrogen, film and anodic dissolution mechanisms for cracking. Preliminary FCP results were reported for alloy 2090 in water vapor[55] and aqueous NaCl[56]. This paper (Part I) reports a detailed characterization of environmental crack growth in 2090. Part II contains a fractographic analysis of corrosion fatigue crack morphologies, as a function of the variables examined in Part I, and a crack tip process zone model based on hydrogen environment embrittlement[57].

III. EXPERIMENTAL PROCEDURE

A. *Material*

Al-Li-Cu-Zr alloy 2090 (38.1 mm thick rolled plate) and Al-Zn-Mg-Cu alloy 7075 (63.5

3Intrinsic environmental fatigue crack growth is defined as that which is solely governed by crack tip mechanical and chemical driving forces and local microstructure; independent of the external influences of closure contact, crack deflection and transient chemical factors.

mm thick plate) were studied. Chemical compositions and mechanical properties are given in Tables 1 and 2. The dissolved hydrogen content of 2090 is between 6.3 and 10.9 weight parts-per-million (ppm) based on vacuum fusion measurements.

Alloy 2090 was obtained in the solution treated and stretched (6%) condition. For aging at 190°C, hardness and 0.2% offset yield strength were maximum after 3 to 5 hours[4]; all fatigue specimens were peak aged for 4 hours before machining. Optical metallography revealed that the microstructure of 2090 contains large flattened grains elongated in the rolling (longitudinal) direction. Average grain sizes in the longitudinal, transverse and thickness directions are 10 mm (or larger), 3.3 mm and 0.11 mm, respectively. The microstructure within each large grain is unrecrystallized and homogeneous through the plate thickness, with sub-grain sizes of 10 μm, 5 μm and 15 μm for the transverse, thickness and longitudinal directions, respectively. The highly textured character of rolled 2090, and the presence of both T_1 and δ' precipitates, are demonstrated in Part II[57]. Alloy 7075 was studied in the T651 peak aged condition.

B. Specimen Geometry

A single edge micro-notched (SEN) specimen (thickness, B = 2.54 mm; width, W = 10.16 mm; and notch depth, a_n = 300 μm) was used to study short fatigue cracks sized between 300 μm and 5 mm. The flat portion of the SEN specimen was 25.4 mm long and transitioned to 10.1 mm diameter round ends, with an overall length of 127.0 mm. The specimen was rigidly threaded into grips which were pin and clevice loaded for unrestricted rotation during crack growth, as required for the bending dominated SEN specimen. A well established stress intensity factor (K) solution was employed for this geometry[58]. Small scale yielding was maintained because applied loads were less than the SEN specimen limit load, and plane stress monotonic plastic zone size was less than 10% of the remaining ligament (W - a) and 15% of the specimen thickness.

Specimens were machined from the plates in the longitudinal-transverse (L-T) and longitudinal-short (L-S) orientations, with the centerline of each specimen located at the 1/3 plate

---

[4]Yield strengths equalled 200, 227, 264, 496 and 482 MPa after aging at 190°C for 0, 1, 2, 3 and 22 hours, respectively.

thickness. For alloy 2090, the scale drawing in Figure 1a illustrates how a short crack propagating in the L-S orientation is embedded within one or two grains; the crack front samples many subgrains and intermittently passes through single high angle boundaries. This L-S case approaches a microstructural small crack geometry[59]; single crack/grain boundary interactions are resolvable. For the L-T orientation, the fatigue crack front continuously samples many (10 to 30) high angle grain boundaries and the subgrain microstructure, Figure 1b. Only the L-S crack orientation was considered for the less anisotropic 7075 plate.

To minimize residual stresses, the micronotch was electrospark discharge machined (EDM). Fatigue crack growth within 30 μm of the notch tip is ambiguously affected by notch bluntness, the notch stress concentration and the brittle melted layer formed by EDM and was not reported[60].

C. *Fatigue Crack Propagation Testing*

The growth of short fatigue cracks was continuously monitored by the direct current electrical potential method[60,61]. Current was input to the specimen through the grips and was maintained constant during cracking to better than $\pm$ 0.05% by a power supply. Potential probes, 0.127 mm diameter copper wire, were spot welded at points centered 0.6 mm above and below the micronotch mouth. For an excitation current of 15 amperes, an initial potential difference of 60 μV (1 μV/amp/cm^2) was measured. This voltage was amplified by 10^4, converted from an analog to digital signal and input to the machine control computer. A computer controlled relay changed the polarity of the applied current to measure and eliminate thermal voltage components to the crack-induced potential. Thermal-corrected and averaged voltage was converted to crack length by a closed form solution to the LaPlacian equation for the voltage field in a cracked infinite plate[62]. Small errors in crack length were linearly corrected based on post-test measurements of the final fatigue crack length. Potential was measured to a precision of $\pm$0.2 μV. Assuming uniform crack growth, crack length measurement resolution was better than $\pm$1 μm.

Fatigue experiments were performed using a closed loop servo-hydraulic test machine operated in load control. A PC-based system provided automated machine control based on measured load and crack length. As crack length increases, load is continuously adjusted to

maintain the programmed ΔK and R. Da/dN was determined by least squares analysis of 20 to 200 crack length-load cycles data points for a minimum steady state crack growth interval of 0.3 mm. ΔK and R were varied, at constant K_{max}, for a single specimen to yield a range of da/dN-ΔK data.

D.   *Environment Control*

Fatigue crack propagation experiments in dynamically pumped vacuum (0.3 μPa) and in static gaseous environments of 2 kPa helium, 20 kPa oxygen and 2 kPa water vapor were performed in a heatable, 10 liter metal bellows and copper gasket-sealed, stainless steel chamber interfaced with a 44.5 kN servohydraulic loading frame. Gas pressure was monitored with either a capacitance manometer or a tungsten filament ion gage for very low pressures. Prior to testing, the chamber was evacuated to below 3 μPa while the chamber walls were degassed at 140°C. Before entry to the vacuum chamber, helium (99.998% pure) was further purified by passage through a molecular sieve at 23°C, followed by a hot titanium alloy chip getter for removal of H_2O, O_2 and H_2. Water vapor was removed from oxygen (99.998% pure) by a dry ice cold trap at low O_2 flow rates. Fatigue loading times were minimized to limit contamination due to chamber degassing. Specimen temperature was monitored by an attached thermocouple.

A 1.5 liter O-ring sealed plexiglass chamber was used for aqueous NaCl corrosion fatigue experiments[54,56]. Specimens were continuously immersed in helium deaerated 1% NaCl (pH = 8) and were maintained at constant electrode potential by a potentiostat, two platinum counter electrodes perpendicular to the SEN specimen faces and a Ag/AgCl reference electrode at the mouth of the notch. Each electrode was isolated from the solution by an asbestos frit to preclude solution contamination. The specimen (working electrode) was grounded, as required for the circuitry of the potentiostat. The NaCl solution was circulated through the plexiglass test chamber, at a rate of 30 ml/min, from a reservoir containing 25 liters of argon deaerated 1% NaCl solution. Only the mid-half of the SEN specimen was contained in the electrolyte, with the chamber design precluding grip metal contact with the NaCl and associated galvanic effects.

The open circuit potentials for peak aged alloy 2090 are -700 mV[5] and -1000 mV for

---

[5] All electrode potentials are stated with respect to the saturated calomel electrode.

air saturated and helium deaerated solutions of 1% NaCl, respectively[54,56]. Based on a breakaway potential of -700 mV for each solution, constant potentials of -840 mV and -1240 mV were selected for corrosion fatigue under anodic and cathodic polarization in deaerated NaCl. Fatigue crack surfaces were not significantly corroded for either potential; only the active T_1 phase locally dissolved[45,54,57].

IV. RESULTS AND DISCUSSION

A. *Crack Length Monitoring and Programmed ΔK-K_{max} Experiments*

The direct current electrical potential method successfully monitored the growth of short fatigue cracks in aluminum alloys exposed to the vacuum, gaseous and aqueous environments of this study. Experiments reported elsewhere demonstrate that: (a) the short edge crack specimen with spot welded potential probes can be fabricated from aluminum alloys, (b) predictions of crack length from measured potentials and the voltage field model differ by less than ±15% compared to optically measured values, for crack lengths between 50 and 5000 μm ahead of the micronotch, (c) the applied direct current has no influence on either electrochemical currents during potentiostatic polarization or on da/dN in NaCl[54]. The results of replicate environmental fatigue experiments for alloy 2090 are in excellent agreement[54].

Crack length and growth rate resolution are excellent. Figure 2 shows a constant ΔK result for alloy 2090 (L-S orientation) in 1% NaCl at a constant anodic potential of -0.840 V. This plot of over 2000 crack length (a) versus load cycles (N) data pairs exhibits a linear slope for crack lengths from 0.3 mm to 4.3 mm and is indicative of intrinsic steady state FCP. Increases or decreases in the slope of this plot represent changes in crack tip mechanical or chemical driving forces due to changes in closure, crack deflection or crack chemistry, and would signify extrinsic fatigue crack growth. Because of the high crack length resolution, shown to be on the order of 1 μm by the insert to Figure 2, small changes in da/dN are resolved.

Steady state corrosion fatigue crack propagation is studied using a procedure based on constant ΔK segments with varying R at constant K_{max}. With a single specimen, the load sequence initially probes high constant ΔK, low R cracking; followed by near-threshold, high R

8

fatigue for deeper crack depths, and ending with several constant ΔK segments at increased R. Each segment is at constant K_{max}. Figure 3 demonstrates constant da/dN at each constant ΔK in this loading sequence for a single specimen of alloy 2090 in moist air. Six of the experiments were performed at a constant K_{max} of 17 MPa/m, while the initial constant ΔK test was performed at a K_{max} of 11 MPa/m to prevent specimen net section yielding. Crack growth at each ΔK extended over about 0.4 mm, with 20 to 100 a-N pairs evaluated for linear response by least squares analysis. There is no evidence of delayed crack growth after any stress intensity range decrease, demonstrating that load shedding at constant K_{max} does not induce retardation, presumably because the maximum or forward loading plastic zone size is constant.

B. *Intrinsic FCP: Alloy 2090 in Moist Air*

The intrinsic fatigue crack propagation behavior of alloy 2090 in moist air is accurately characterized by the short crack, constant ΔK and K_{max} step changed R method. The results in Figure 4 were determined from the loading sequence and crack length data of the type presented in Figure 3. Two specimens were employed for each of the L-T and L-S orientations. For R less than 0.7, mildly decreasing da/dN with increasing crack length indicated crack closure and therefore extrinsic FCP. To better estimate intrinsic behavior, the applied ΔK was reduced by less than 15% for these cases[54]. The results in Figure 4 agree with 2090 literature FCP data which are not affected by crack closure, including replication based microstructurally small crack kinetics[6] and high stress ratio growth rates[18,52]. Short crack data for the L-T orientation agree with the results from a continuously decreasing ΔK/increasing R experiment with a compact tension (CT) specimen at constant K_{max} (17 MPa/m), as shown by the insert[54,55]. This specimen was machined from the plate of alloy 2090. In contrast to the short crack results, the CT data in Figure 4 were not corrected to account for crack closure. The CT and short crack results agree exactly if the latter are not correlated based on ΔK_{eff}[54,55]. Since the CT data most likely reflect a closure influence at R less than about 0.7, the short crack data in Figure 4 better define the intrinsic FCP behavior of peak aged 2090 in moist air.

Figure 4 shows identical intrinsic FCP behavior for the L-S and L-T orientations of alloy 2090, confirming that orientation effects on da/dN at low R are due to crack closure[18-21]. The intrinsic growth rates for alloy 2090 are essentially equal to da/dN-ΔK data for a wide variety

of aluminum alloys examined at high stress ratio[18]. Similar da/dN for the single grain/L-S and multiple grain/L-T orientations establish that high angle grain boundaries do not affect transgranular fatigue crack growth rates for 2090 in moist air. Crack growth retardation or arrest by such boundaries in the L-S orientation were never observed. These results are at odds with surface replication studies of small cracks in single grains of aluminum alloys, where the grain boundary causes crack growth retardation and arrest[54,59,61].

The da/dN-ΔK response for alloy 2090 in moist air exhibits three regimes of behavior: (a) Paris-Law cracking at moderate ΔK, with a power-law exponent on the order of 3.7, (b) no evidence of a crack growth threshold, ΔK_{th}, for high R and da/dN as low as 10^{-7} mm/cycle, with a second power-law relationship observed, and (c) transition or "plateau" behavior at moderate ΔK, where there is little change in da/dN as ΔK ranges from 4 MPa$\sqrt{}$m to 7 MPa$\sqrt{}$m. The three region behavior shown in Figure 4 is physically real and reproducible. Single da/dN-ΔK points are the result of linear regression of substantial crack length data. The same da/dN-ΔK relationship is indicated for each orientation of alloy 2090 and the three region response is confirmed by the long crack compact tension experiment (L-T orientation) with continuously decreasing ΔK at constant K_{max}[54,55]. The origin of the da/dN-ΔK relationship in Figure 4 is discussed in an ensuing section (IV.E.1).

C. *Intrinsic FCP: Alloys 2090 and 7075 in Purified Gaseous Environments*

Constant ΔK and K_{max} short crack FCP experiments were performed on peak aged 2090 (L-S and L-T) and 7075 (L-S) in water vapor, helium, oxygen and vacuum at a frequency of 5 Hz. For 2090, L-S orientated fatigue cracks exhibited severe out-of-plane cracking in helium and vacuum because of the crystallographic slip plane cracking mode and a strong texture, as discussed in Part II[57]. Crack length measurement accuracy was adversely affected by crack surface electrical contact[61] and growth rates are not reported. For purified oxygen, "crack surface shorting" was not observed; L-S and L-T intrinsic FCP rates for 2090 were identical.

1. *Inert and Water Vapor Environments*

Alloy 2090 (L-T) FCP results are presented in Figure 5 for a constant K_{max} of 17 MPa$\sqrt{}$m and compared to data for moist air, plotted as the dashed line from the L-T results in Figure 4.

At high ΔK (> 10 MPa√m) and low R (0.05), the FCP rates in 2090 are equal for exposure to helium, water vapor and moist air. These data suggest no resolvable environmental effect on da/dN at high crack growth rates and are consistent with a Paris exponent of 4.0. Equivalent and slow crack growth rates are observed for 2090 in the helium and dynamic vacuum environments as ΔK is reduced to near-ΔK_{th} at increasing R. A single Paris-law behavior is observed with an exponent of 4.0, particularly for the purified helium environment.

Initial experiments with helium suggested that part-per-million levels of contamination, presumably water vapor, affect FCP rates[54,55]. The use of molecular sieve and hot titanium alloy chips to further purify He emerged from this experience. Contamination originated from the vacuum chamber walls when the gas environment was stagnantly maintained without replenishment. To minimize this problem, fatigue experiments were conducted over limited times and with gas exchanges between constant ΔK segments. Data for He were compared to growth rates in dynamically pumped vacuum at better than 1 μPa. The good agreement for such data in Figure 5, and the linearity of a versus N (or time) at constant ΔK, confirm this purification procedure. When contamination was not controlled, crack growth rates in He varied with cycling time at constant ΔK and approached the values typical of 2 kPa water vapor.

In contrast to the "inert" environments, pure water vapor and moist air increase low ΔK crack growth rates in 2090 by up to 10-fold, without evidence for a threshold stress intensity. The two growth rates for water vapor are consistent with a $\Delta K^{4.0}$ relationship and the value at the lowest ΔK level is above that for moist air. Figure 5 indicates "plateau" or transition da/dN-ΔK behavior for purified water vapor, similar to FCP in moist air. The single power-law da/dN-ΔK relationship for 2090 in the two inert environments indicates that transition behavior is not solely based on microstructural effects. Rather, the importance of environment is indicated.

Gaseous environmental effects on FCP in alloy 7075 are shown in Figure 6. Similar da/dN are observed for alloys 7075 and 2090 in helium and dynamic vacuum, particularly at ΔK levels above about 8 MPa√m. At lower ΔK, da/dN are somewhat faster for 2090 compared to 7075, perhaps due to localized planar slip in ordered δ' strengthened 2090[19]. Insufficient work has been done here or elsewhere to clearly define the plasticity dominated intrinsic FCP behavior of various aluminum alloys in inert environments.

The da/dN-ΔK data in Figure 6 indicate that 7075 is more strongly affected by "high

pressure" (2 kPa) water vapor compared to 2090. At high ΔK 7075 exhibits a factor of three increase in da/dN for water vapor compared to helium, while 2090 is not environment sensitive. For near-ΔK_{th}, the da/dN value for 7075 in water vapor is a factor of ten faster than that observed for 2090. Alloy 2090 exhibits a ten-fold increase in da/dN for 2 kPa water vapor compared to helium and vacuum, while alloy 7075 exhibits a factor of 100 increase.

Water vapor enhanced FCP in aluminum alloys is generally attributed to hydrogen embrittlement[23,25,26-30,37-40]. Atomic hydrogen, produced by water vapor reactions with clean crack surfaces of aluminum, adsorbs at the crack tip and may transport into the plastic zone ahead of the crack tip to enhance da/dN. To confirm this hypothesis for Al-Li-Cu alloys, it is necessary to examine possible embrittlement due to oxygen and oxide films, and to probe variables (viz., water vapor pressure) which affect hydrogen environment embrittlement.

2. Oxygen/Oxide Film Effects

The results in Figure 7 demonstrate that purified gaseous oxygen does not affect FCP in 2090; equal growth rates are observed for O_2, He and dynamic vacuum. Compared to helium, mildly reduced da/dN are observed for 2090 in oxygen at ΔK between 6 and 11 MPa$\sqrt{m}$ for low R. Fractographic examination revealed that this behavior is most likely due to oxide debris induced crack closure[54,57]. Equivalent and slow crack growth rates are observed for alloy 2090 in oxygen, helium and dynamic vacuum as ΔK is reduced to near-threshold at increasing R. Intrinsic FCP in 2090 in O_2 is well described by the single power-law relationship between da/dN and $\Delta K^{4.0}$ determined for cracking in helium.

Auger electron spectroscopic analysis of ion sputtered 2090 fatigue crack surfaces confirmed that a substantial oxide film formed during cyclic loading in O_2 compared to He or vacuum[54]. A thicker oxide film was formed in O_2 at low R compared to high R, consistent with a fretting mechanism[17]. These results agree with Auger and SIMS studies which revealed oxide formation and possible atomic oxygen transport into the crack tip process zone during fatigue of aluminum alloys in O_2[63]. The lack of an O_2 effect on da/dN for alloy 2090 suggests that the surface oxide film does not influence fatigue damage by either preventing reversible slip, and thus increasing da/dN[19,42,64,65], or by homogenizing localized deformation, and thus decreasing da/dN[27].

12

The effect of oxygen on FCP in aluminum is clouded when 7075 and literature data are considered[23]. Figure 7 compares intrinsic da/dN for 7075 (L-S) and 2090 (L-T) stressed in oxygen, helium and vacuum. At high ΔK (> 10 MPa/m) and low R, little difference is observed in the growth rates for either alloy in either environment, suggesting that oxygen is not damaging. These results agree with reports of similar crack growth kinetics for 7075 and 2219 in O_2 and vacuum at moderate ΔK and low R[63,66]. The results in Figure 7 contradict data which indicate two-fold slower growth rates for 7075 in oxygen compared to argon or vacuum at ΔK above 6 MPa/m[27]. Oxide induced crack closure in the long crack compact tension specimen may have played a role in these latter results. At low ΔK, 7075 cracks at increased rates in oxygen compared to vacuum, in contrast to 2090. Bradshaw and Wheeler demonstrated a similar strong effect of O_2 on fatigue of a 7000 series alloy[30]. They reported that oxygen either had no effect, or slightly retarded crack growth rates compared to vacuum for ΔK levels above 6 to 8 MPa/m; O_2 enhanced da/dN by over an order of magnitude at lower ΔK. Crack growth rates decreased with decreasing oxygen pressure and growth was faceted along slip bands for vacuum, while a flat "tensile" mode of unspecified morphology was observed for O_2.

Interpretation of O_2 effects on FCP is hindered by two problems. The rough crack surface typical of fatigue in vacuum, and oxidation debris of thickness on the order of 0.1 to 1 μm, cause crack closure. The Bradshaw and Wheeler data can be interpreted based on oxide induced closure for O_2 at moderate ΔK and faceted surface roughness induced closure for vacuum at low ΔK. Near-threshold faceted cracking and surface roughness could decrease, and da/dN could increase, with increasing oxygen pressure. Closure does not explain the crack path transition. Secondly, despite precautions to purify O_2[54,55], the high R results for 7075 in Figure 6 may be attributed to water vapor contamination of the static oxygen environment. The O_2 effect is only demonstrated for alloy 7075 which is thought to be sensitive to hydrogen embrittlement[27]. The subtle growth rate plateau for alloy 7075 in oxygen (Figure 7) suggests a water vapor effect; similar to that observed for 2090 in water vapor and moist air (Figure 5).

For similar purity oxygen environments, reduced intrinsic fatigue crack growth rates are indicated in Figure 7 for alloy 2090 compared to 7075. If water vapor was present in each O_2 environment, this result suggests that a given amount of hydrogen is more embrittling to the 7000 series alloy compared to 2090. Alternately, oxygen may form a more protective surface film

13

which competes with water vapor in alloy 2090. Research is required to examine the effect of oxygen on intrinsic fatigue in aluminum alloys. From the present study, however, there is no evidence to indicate that pure O_2 enhances FCP rates for alloy 2090; the deleterious effect of water vapor is more reasonably traced to hydrogen embrittlement.

3. *Effect of Water Vapor Pressure*

This section demonstrates the water vapor pressure dependence of da/dN for alloy 2090 and provides evidence for the hydrogen embrittlement mechanism for FCP. The results in Figure 8; da/dN versus water vapor pressure (P_{H2O}) for L-T 2090 at constant ΔK of 2.4 MPa√m, R of 0.86 and frequency of 5 Hz; are consistent with data and hydrogen embrittlement modeling by Wei and coworkers for 2000 and 7000 series alloys[25,27,28,40]. Specifically, crack growth rate is independent of P_{H2O} above a so-called saturation pressure of 0.2 Pa. Da/dN is reduced by a factor of ten as P_{H2O} is lowered below the saturation pressure and growth rates approach the level typical of inert gases and vacuum. Within this regime for alloy 2090, da/dN is proportional to P_{H2O} raised to the 0.25 power. Literature results for 2219 and 7075 indicate a stronger pressure dependence, with an exponent of 0.6[27,28].

According to the hydrogen embrittlement model, because aluminum alloy surface reactions with water vapor are rapid, the rate of crack tip hydrogen production is governed by impeded molecular (Knudsen) transport of H_2O in the fatigue crack[28]. Water molecule-crack wall interactions, rather than intermolecular collisions, govern mass transport to the crack tip. Below the H_2O saturation pressure (< 0.2 Pa for alloy 2090 at R = 0.86), decreasing bulk environment gas pressure (or increasing loading frequency) results in decreased hydrogen production, because less water vapor is provided to the crack tip, and corrosion fatigue crack growth rate decreases. At or above the saturation pressure, the aluminum-water vapor surface reaction progresses to completion and is independent of further increases in crack tip P_{H2O} (or loading time); accelerated corrosion fatigue crack growth rates are constant. This model qualitatively explains the data in Figure 8; hydrogen embrittlement is implicated for 2090 in water vapor.

For aluminum alloys loaded at moderate ΔK, low R less than 0.5 and a loading frequency of 5 Hz, saturation pressures of 1 to 10 Pa are indicated[27,28]. Alloy 2090 data in Figure 8, for

low ΔK and high R, indicate an order of magnitude reduction in this pressure to 0.2 Pa. The data for lithium bearing 2090 are unique to the near-threshold regime, and a variety of mechanisms could be proposed to explain the strong effect of very low water concentrations[55]. Knudsen flow modeling indicates, however, that the low saturation pressure is due to high R and the associated crack opening. As the mean crack opening increases, crack wall impedance to water vapor transport decreases and crack tip P_{H2O} increases. Specifically, Shih and Wei predict that the saturation pressure is inversely proportional to a function of R ($f(R)$ = $\{[(1+R)/(1-R)]^2$ + 0.5\}/4.0) and is directly proportional to $(E/\sigma_{ys})^2$ [25]. Figure 9 contains their data on the saturation pressure for alloy 2219 at moderate ΔK and R < 0.5, along with the high R (0.86) result for 2090 and low R-moderate ΔK literature data for 5070 and several 7XXX alloys[25,27,30,68,69]6. The least squares line for all data has a slope of 0.7, in reasonable agreement with the predicted slope of 1.0 from the Knudsen flow model[25]. The low saturation pressure for 2090 is the result of the high stress ratio employed to define intrinsic FCP. This result supports the hydrogen embrittlement mechanism for cracking in water vapor.

The data in Figures 8 and 9 establish that extremely low levels of water vapor, 1 to 10 ppm by pressure in the inert helium gas, enhance fatigue crack growth in alloy 2090 for high R and near-ΔK_{th} loading. This fact further supports hydrogen embrittlement from a number of perspectives. First, at such low H_2O pressures, cracking by capillary condensation of water and electrochemical dissolution mechanism is unlikely. This conclusion is established from the Kelvin equation, which approximates the external pressure at which crack tip condensation would occur on a curved surface[67], coupled with a continuum mechanics description of the blunted crack tip radius (radius, ρ, equals $K^2/4\sigma_{ys}E$). These calculations indicate that, for an external P_{H2O} of 0.01 Pa, water only condenses within the crack tip region when the applied stress intensity during the fatigue cycle is less than 4.5 MPa$\sqrt{m}$ to reduce ρ below 0.15 μm. This low K level was never reached during high R cracking; as such, accelerated crack growth in 0.01 Pa water vapor is not due to condensed water.

A complex crack tip geometry may result from local buckling during unloading, crack

---

6Water vapor transport and crack growth rate are controlled by an exposure parameter which is the ratio of water vapor pressure to loading frequency[40]. Experiments with 2090 were at a constant frequency of 5 Hz, however, the literature data in Figure 9 were obtained for a variety of frequencies necessitating the use of the exposure parameter.

15

tip deformation mode and cracking along crystallographic planes. Here, water condensation may be more likely. The possibility of accelerated crack growth by dissolution is, none-the-less, remote. The kinetics of condensation and the formation of an electrolyte are not understood, and cannot be assumed as favorable for dissolution. ΔK dependent changes in fracture mode suggest a process zone volume mechanism for crack growth, as discussed in Part II[57]. Dissolution-based cracking is localized to the crack-environment interface.

Figures 8 and 9 explain why extremely small levels of water vapor contamination enhance rates of high R near-ΔK_{th} FCP in aluminum alloys, including 2090, exposed to presumably benign vacuum, helium or nitrogen[17,29,50,55]. It is difficult to eliminate such low water vapor pressures and truly inert environments are difficult to establish. For experiments with low R and moderate to high frequency (for example R = 0.1 and f above 10 Hz), water vapor does not transport to the crack tip in sufficient quantity to influence da/dN. Contamination effects on da/dN for vacuum or inert gases are less likely.

D.   INTRINSIC FCP: ALLOY 2090 IN AQUEOUS ENVIRONMENTS

Aqueous NaCl enhances rates of fatigue crack growth in 2090, with the magnitude of the environmental effect depending on ΔK, frequency, anodic or cathodic polarization, and Li_2CO_3 addition. Hydrogen embrittlement is implicated. Faster crack growth is correlated with those environmental conditions which may destabilize crack surface films and therefore enhance the efficiency of hydrogen entry at the crack tip.

Figure 10 presents the results of constant ΔK and K_{max} intrinsic FCP experiments, performed on peak aged L-T 2090 SEN specimens in deaerated 1 wt% NaCl and 1% NaCl + 0.4% Li_2CO_3. Da/dN-ΔK data are included for 2090 in helium and moist air. The aqueous chloride results were obtained from several specimens loaded at a constant frequency of 5 Hz and electrode potentials of either -0.840 V (anodic polarization) or -1.240 V (cathodic). Considering anodic polarization and high ΔK-low R ($\Delta K > 10$ MPa/m and R < 0.1), alloy 2090 exhibits a factor of two increase in da/dN compared to the inert and water vapor environments. The largest environmental effect is observed for lower ΔK at high R; 1% NaCl with anodic polarization causes up to a fourteen-fold increase in da/dN compared to helium. If ΔK_{th} exists, NaCl reduces the value to less than 1 MPa/m. Cathodic polarization at -1.240 V reduces fatigue

crack growth rates to levels typical of moist air, and produces an apparent threshold above the moist air value and similar to helium. Plateau behavior was not observed for FCP under anodic polarization, however, a mild growth rate transition is indicated in Figure 10 for cathodic polarization. Similar to the water vapor case, peak aged 2090 exhibits better aqueous chloride fatigu crack growth resistance compared to 7075-T651. For high ΔK and 1% NaCl at -0.840 mV, the L-S crack orientation of 7075 exhibits up to a 7-fold increase in da/dN compared to helium and a 3-fold increase compared to 2090 in NaCl. Larger increases in da/dN are observed for environmental cracking of 7075 in the low ΔK regime.

For anodically polarized alloy 2090 (-0.840 V), the addition of 0.4% Li_2CO_3 to 1% NaCl retards crack growth rates at constant pH of 10.4; Figure 10. The magnitude of the Li_2CO_3 effect was confirmed by constant ΔK experiments which resolve 15% changes in da/dN in response to an environmental change while the fatigue crack propagates[54,56]. These experiments indicated that increased pH of bulk 1% NaCl, from 8.1 to 10.4 by sodium hydroxide addition, had no influence on da/dN. A subsequent Li_2CO_3 addition to NaCl at pH 10.4 and constant electrode potential mildly reduced da/dN. Gui and Devine demonstrated that lithium ions in aqueous solution passivate aluminum, with the film being stable in the presence of Cl^- ions[70]. It is postulated that Li_2CO_3 forms a protective passive film on the 2090 fatigue crack surface, resulting in reduced da/dN by hindering hydrogen uptake as considered in Part II[57]. A surface film should not mechanically influence da/dN based on the FCP data for the O_2 environment; Figure 5.

1. *Effect of ΔK*

The data in Figure 10 demonstrate that environment governs the relationship between da/dN and ΔK. The fatigue crack growth rate law, be it a simple power-law or a complex sigmoidal function, may be influenced by mechanical factors. Crack closure strongly affects da/dN[18], however, this mechanism is not relevant to the data in Figure 10 because of the underlying experimental method. The slope of an intrinsic power-law will increase at high ΔK due to static mode cracking as K_{max} approaches the pertinent fracture toughness, K_{IC}, K_c or K_{ISCC}. The data in Figure 10 are not affected by static mode cracking because K_{max} is constant (17 MPa√m) for all ΔK, and is well below K_c and K_{ISCC}. The plane strain fracture toughness

(K_{IC}) for 2090 peak aged at 190°C is 30 MPa√m[8], however, a single compact tension experiment during the current study indicated that K_{IC} may be as low as 21 MPa√m. Since the 2.5 mm thick SEN specimens deform under substantial plane stress for K levels above 20 MPa√m, the critical inert environment toughness (K_c) relevant to Figure 10 is 30 to 40 MPa√m. Considering NaCl, reliable K_{ISCC} data are not available for L-T peak aged 2090. Static load environmental cracking is, however, unlikely at electrode potentials below -700 mV$_{sce}$[16,46,71]. This speculation is confirmed by FCP experiments with varying loading frequency, as described in the next section.

Yoder et al. and Wanhill argue that the slope of the da/dN-ΔK relationship transitions at low ΔK when the cyclic plastic zone size is equal to a microstructural feature which governs slip deformation (e.g., grain size)[72-75]. This mechanism is not supported by the data in Figure 10. A single power-law relationship ($\Delta K^{4.0}$) is observed for 2090 in inert helium, and to a lesser extent for oxygen and vacuum; cyclic plastic zone diameter is as small as 0.5 μm, while subgrain and high angle grain sizes are one to three orders of magnitude larger. Yoder and coworkers developed the microstructural model based on FCP data for moist air, but did not consider the environmental influence.

Complex relationships between da/dN and ΔK are exclusively observed for 2090 in the aggressive environments of NaCl, moist air and water vapor; Figure 10. Two power-law, transition plateau behavior is observed for moist air, NaCl with cathodic polarization and water vapor (Figure 5), and for 7075 in contaminated O_2 (Figure 7). A single low ΔK transition occurs for 2090 in NaCl with anodic polarization. Crack arrest at ΔK_{th} was not observed for the environments represented in Figure 10, with the possible exception of NaCl with cathodic polarization. Additional data are required to establish threshold behavior. The dominant role of environment on da/dN-ΔK is supported by data for 2000 and 7000 series aluminum alloys in moist air, water vapor and NaCl[24,26,32,34,76].

The data in Figure 10 were obtained for constant K_{max} and increasing mean stress with decreasing ΔK to minimize crack closure. Mean stress intensity may affect the intrinsic relationship between da/dN and ΔK. The simple power-law observed for the inert environments, and the similarities between da/dN-ΔK for 2090 and less closure-prone aluminum alloys in aggressive environments indicate that the results in Figure 10 are not uniquely affected by R.

This issue, which has not been addressed in the literature, will be investigated by modeling in Part II and in a future study.

Complex da/dN-ΔK relationships in environmental fatigue have been recognized, without sufficient mechanistic explanation or modeling[23,40,77]. Feeney et al. argue that environmental growth rates transition to the inert environment power-law relationship when K_{max} is sufficient for plane stress, a stress state that is unfavorable for hydrogen embrittlement[24]. This explanation is not likely for the stress intensities represented in Figure 10. K_{max} is constant for all ΔK, cyclic plastic zone sizes are small compared to specimen thickness, and slanted fatigue crack surfaces were not observed. Transitions at low ΔK were recognized, but not explained and may have been caused by crack closure[24]. Several workers argue that the environmental effect is eliminated at high ΔK because mechanical crack growth is faster than the rate limiting step in the mass transport and chemical reaction sequence which supports environmental cracking[26,32,34,76]. An example is hydrogen diffusion limited crack growth[32,34]. The cause of the lower ΔK transition, and the associated plateau, is not understood.

Fractographic results and a process zone hydrogen cracking model presented in Part II demonstrate that the ΔK dependence of da/dN is determined by the interaction of cyclic strain defined process zone size (ΔK), crack tip normal stress (K_{max}), unrecrystallized subgrain size, crack surface hydrogen production, and process zone hydrogen concentration (entry)[57].

2. Effect of Loading Frequency

From the hydrogen embrittlement perspective, environmental FCP rates are expected to increase with decreasing loading frequency (f), or to exhibit time independent saturation behavior, mirroring the time dependencies of crack environment mass transport, local hydrogen production and process zone diffusion[23,40]. The expected frequency effect is not observed for peak aged alloy 2090 in NaCl, as established by short crack data for the L-T orientation in aqueous NaCl with anodic polarization (-0.840 V) and at two levels of constant ΔK. Figure 11a shows that da/dN increases by a factor of two as f increases from 0.1 Hz to 5 Hz for a constant ΔK (9.9 MPa$\sqrt{m}$ at R = 0.1). No systematic change in da/dN was observed for low ΔK, high R (2.2 MPa$\sqrt{m}$ and 0.8) loading at frequencies ranging from 0.07 to 20 Hz. The numbers adjacent to each data point describe the frequency sequence conducted on a single specimen at

ΔK. For each frequency, the total variation in crack growth rate with increasing crack length (calculated with a two point secant method) and the least squares average value are plotted in Figure 11a. Some variability in the da/dN versus f response is observed at low ΔK; electrical potential system variations over the several-day term of the low frequency experiments probably caused this behavior. The frequency effects shown in Figure 11 were confirmed by additional experiments[54]. For example, the constant ΔK crack length data in Figure 11b demonstrate small differences in steady state corrosion fatigue crack growth rate as a function of f.

Yoder and coworkers reported a small effect of frequency on da/dN for alloy 2090 in aerated 3.5 wt% NaCl during free corrosion[48]. Crack growth rates were marginally slower at 0.1 Hz compared to 5 Hz for ΔK between 8 and 20 MPa√m at low R. In contrast extensive results, mainly for environment sensitive 7000 series alloys in aqueous NaCl, indicate that da/dN increases with decreasing frequency for 7017[32], 7475[34], 7175[78], 7075[79], and 2618[78], at ΔK levels above 5 MPa√m (7475), 12 MPa√m (7017 and 7075) and 8 MPa√m (2618 and 7175) at low R. While 2618 and 7175 exhibited equal (saturation) growth rates at 0.1 and 1 Hz compared to lower da/dN at 25 Hz, rates for 7017 and 7475 continuously increased with decreasing frequency according to a $1/\sqrt{f}$ dependence[32,34]. These studies indicate that the frequency effect diminishes for ΔK below 4 to 8 MPa√m, however, no systematic studies of near-ΔK_{th} time dependencies exist.

Interpretation of the frequency effect shown in Figure 11 is not possible until an integrated hydrogen production and crack tip damage model is developed. Qualitatively, such trends do not preclude a hydrogen embrittlement mechanism for environmental fatigue. Increased Paris regime crack growth rates with increasing frequency, and no resolvable low ΔK frequency effect, suggest that mass transport within the electrolyte, chemical surface reactions and the crack tip plastic zone hydrogen diffusion do not limit da/dN. Speculatively, a protective surface film is destabilized with increasing frequency and therefore crack tip strain rate; time based hydrogen production and uptake increase and promote FCP. That is, since da/dN equals da/dt times 1/f, average crack advance per unit time (da/dt) increases with increasing frequency or crack tip strain rate more strongly than 1/f decreases.

Considering the lack of a frequency effect at low ΔK, the level of average crack tip plastic strain rate is substantially less than that of the high ΔK case and may not be sufficient for

repeated film rupture. Average crack tip strain rate during the loading portion of a fatigue cycle is approximated by $\phi\Delta K^\gamma f$, where γ is a constant between 2 and 6, and ϕ is a proportionality constant[23]. Davidson and Lankford reported that γ varies between 2.5 and 3.5 for 7075 in moist air[80,81]. For γ equal to 3.0, f levels between 10 and 200 Hz are required to develop film destabilizing near-ΔK_{th} (2 MPa√m) crack tip strain rates equivalent to those produced at higher ΔK (10 MPa√m) at 0.1 < f < 2 Hz. Such high frequencies were not examined, Figure 11a, precluding direct comparison of the frequency effects in these two ΔK regimes. Chemical reaction and mass transport may limit da/dN at high frequencies and further complicate the effect of frequency[40].

Additional work is required to explain the effect of frequency on surface film stability, electrochemical reactions and hydrogen transport within the alloy. For example, the effect of localized planar slip deformation on crack tip strain rate must be defined. Discontinuous versus per cycle cracking and the possibility of different microscopic modes of hydrogen damage at low and high ΔK must be examined. The importance of these issues is confirmed in Part II[57].

3. *Effect of Applied Electrode Potential*

The results in Figure 10 for NaCl indicate that cathodic polarization substantially reduces fatigue crack growth rates in 2090 relative to the free corrosion potential. This beneficial effect was reproduced by constant ΔK experiments. Low ΔK (2.2 MPa√m at R = 0.8) results are presented in Figure 12. Da/dN is constant at an anodic potential of -0.840 V and over a crack length interval of from 0.3 to 2.1 mm.[7] Here, application of a mild cathodic potential (-1.240 V) resulted in crack arrest, consistent with the data in Figure 10. After 10^6 cycles at -1.240 V, without resolvable crack growth, the specimen potential was changed to -0.840 V. After 76 hours of exposure, accumulating 2.2 million load cycles at constant ΔK, crack growth resumed and achieved a steady state rate similar to the initial anodic condition. A second polarization of -1.240 V reproduced crack arrest. Experiments performed at high ΔK (10 MPa√m at R = 0.1) show that greater cathodic potential (-1.340 V) is required to reduce da/dN[54]. Fractographic analysis of the low ΔK cathodically arrested crack revealed no evidence of crack tip blunting.

---

[7]The loading frequency effect represented in Figure 11 was characterized during this portion of the experiment.

Arrest markings were shallow and barely visible at a magnification of 5,000 times, with no evidence of enhanced dissolution or pitting. The fracture surfaces which were cathodically polarized exhibited a black surface film, presumably a hydroxide based phase[82]. This film also formed *in situ* about the intersections of the crack edges and the specimen surface.

The beneficial effect of cathodic polarization on environmental FCP in 2090 is consistent with the behavior of other aluminum alloys. Paris regime da/dN increase with anodic polarization and decrease with cathodic potentials for Al-7 wt% Mg in Na_2SO_4[41], alloy 5086 in seawater[83] and alloy 7075 in NaCl[31]. Mild cathodic polarization reduced da/dN to levels near those observed for moist air or impure argon and affected a brittle-to-ductile transition in the microscopic crack path[31]. A similar beneficial effect of cathodic polarization was reported for monotonic load cracking of 2000 and 7000 series alloys[22,84], and corrosion fatigue crack growth above K_{ISCC}[32].

Hydrogen embrittlement can govern crack growth, despite this intuitively contradictory result. In addition to increasing the rates of proton and water reduction reactions, cathodic polarization affects the crack potential gradient, local pH and surface films[23]. Speculatively, transient crack growth rates after changes in potential and fractographic results suggest a beneficial surface film effect on hydrogen uptake. The low ΔK result in Figure 12 shows that, after changing to an anodic potential, over 2 million load cycles are required to reinitiate crack growth. It is speculated that mechanical damage penetrates the cathodic surface film before anodic crack growth rates are reestablished. The long delay between steady state cathodic and anodic behavior appears to be inconsistent with a crack chemistry transient. There is also no evidence that the crack tip blunted due to corrosion during cathodic polarization, an otherwise reasonable explanation for the prolonged fatigue incubation time.

4. *Effect of Alloy Composition and Microstructure*

Alloy 2090 exhibits good resistance to fatigue crack propagation in aqueous chloride, similar to the results for water vapor. Lithium *per se* does not render 2090 abnormally active to environmental embrittlement for the L-T and L-S orientations. The increased sensitivity of 7075 compared to 2090 for water vapor (Figure 7) and NaCl (Figure 10), but not the inert environments (Figure 6), is consistent with the well known high stress corrosion cracking and

corrosion fatigue resistance of 2000 compared to 7000 series alloys[22,23,84]. The mechanism for this effect is unclear. Lin and Starke argue that copper reduces da/dN by reducing precipitate coherency and the degree of localized planar slip which promotes hydrogen embrittlement[35]. Alternately, magnesium, segregated at grain boundaries in 7000 alloys, is proposed to exacerbate hydrogen embrittlement by affecting surface reaction kinetics[85]. This argument is controversial[86]. The effectiveness of grain and subgrain boundary precipitates as deleterious hydrogen traps may vary with alloy composition[57].

The short crack experiments performed on peak aged alloy 2090 indicate that high angle grain boundaries do not affect FCP in aqueous chloride. This result is analogous to that for 2090 in moist air, Figure 4, and is supported by fractographic analyses[57]. For through thickness edge cracks in deaerated 1% NaCl (-0.840 V), similar intrinsic growth rates are observed for L-T/multiple grain and L-S/single grain crack orientations. The two constant ΔK results plotted in Figure 13 for the L-S orientation (■) are consistent with the da/dN-ΔK response for the L-T/multiple grain data (*). The constant ΔK results in Figure 2 for 2090 in NaCl reveal that the average da/dN is constant as the crack propagates through single grains and interacts with high angle grain boundaries in the L-S orientation. The specimen was metallographically sectioned parallel to the crack growth direction to reveal the microstructure below the fatigue fracture surface. The location of each high angle grain boundary is indicated by arrows in Figure 2. Based on grain size, and since crack tip tunneling was not observed, the crack front intersected one to three grain boundaries as it propagated in the L-S orientation. Little variation in the slope of the a versus N plot shown in Figure 2, with 1 μm resolution, and no evidence of localized corrosion suggest that high angle grain boundaries do not effect transgranular crack propagation in aqueous NaCl.

5. *Chemical Crack Size Effects*

Experiments with a martensitic steel in aqueous chloride establish that fatigue crack growth rates are greatly enhanced for short (150 μm to 5 mm) crack lengths and restricted mouth openings compared to long (5 to 50 mm) cracks[23,40,44,53]. The mechanism for this breakdown in ΔK-similitude is chemical, based on crack geometry sensitive changes in crack chemistry and hydrogen production. The crack size variable has not been considered for aluminum alloys.

The constant ΔK results in Figure 2 reveal no evidence of crack length effects for alloy 2090 in aqueous NaCl; da/dN is constant while crack length increases from 0.3 mm to 4.3 mm. Da/dN was constant with crack growth for all constant ΔK experiments conducted with alloy 2090 in aqueous NaCl. The results in Figure 13 demonstrate equivalent growth rates for short cracks (0.3 mm to 4 mm) and long cracks (20 to 50 mm) in 2090 and 7075 exposed to NaCl[31,47-50]. For Paris regime and near-threshold, short fatigue cracks (a < 1 mm) in 2090 in deaerated 1% NaCl (-0.840 V) grow at similar rates compared to long cracks in aerated 3.5% NaCl at open circuit potentials. For alloy 7075, short cracks (a < 1 mm) grow at somewhat reduced rates compared to long cracks in 3.5 % NaCl for potentials near -0.840 V.

V. CONCLUSIONS

1. Intrinsic fatigue crack propagation (FCP) rates in peak aged Al-Li-Cu alloy 2090 are not affected by highly purified helium, vacuum and oxygen environments. Growth rates (da/dN) are accelerated, particularly at low ΔK and in order of decreasing magnitude, by aqueous 1% aqueous NaCl with anodic polarization, pure water vapor, moist air and NaCl with cathodic polarization.

2. Alloy 2090 exhibits better intrinsic environmental FCP resistance compared to 7075-T651, a conventional aerospace aluminum alloy, and similar to other 2000 series alloys.

3. Hydrogen embrittlement is implicated as the causal mechanism for environmental fatigue cracking of 2090 in moist air, water vapor and aqueous chloride. Surface oxide, from O_2 and presumably water vapor reactions with aluminum, has no effect on intrinsic da/dN in alloy 2090, however, the FCP behavior of 7075 in O_2 is unclear.

4. While FCP rates above 10^{-7} mm/cycle depend on $\Delta K^{4.0}$ for 2090 in helium, vacuum and O_2, multiple da/dN-ΔK power-laws and transition "plateau" behavior are hydrogen environment induced for water vapor and NaCl. Such transitions suggest ΔK dependent

environmental crack tip damage mechanisms.

5. Low ΔK, high K_{max} fatigue crack growth in 2090 is enhanced by part-per-million levels of water vapor at pressures below that necessary for capillary condensation. The H_2O pressure dependence of da/dN, and the decrease in "saturation pressure" with increasing mean crack opening, agree with the predictions of an impeded molecular transport model and support hydrogen embrittlement.

6. Environmental FCP rates are decreased by chemical or loading conditions that favor a stable crack surface film which reduces hydrogen uptake. Da/dN in the 2090/NaCl system decreases with decreasing loading frequency, upon the addition of passivating ions (Li_2CO_3), and with mild cathodic polarization. Crack arrest, produced by cathodic polarization, requires anodic potential and prolonged cyclic loading for reinitiation.

7. The FCP behavior of alloy 2090 in moist air and in NaCl is independent of crack orientation (L-T and L-S) in rolled plate. Small cracks in single grains do not grow at unexpectedly high rates and are not arrested by grain boundaries.

8. ΔK-based similitude describes crack growth rates for 2090 and 7075 in NaCl, independent of crack size between 300 μm and 50 mm.

9. The steady state, intrinsic FCP behavior of aluminum alloys is accurately characterized by direct current electrical potential monitoring of short cracks with programmed constant ΔK and K_{max} loading for vacuum, gaseous and aqueous environments.

VI. ACKNOWLEDGEMENTS

Colvin of the Alcoa Technical Center. J.A. Wert, G.E. Stoner, E.A. Starke and M.F. Henry provided important inputs. These contributions are gratefully acknowledged.

VII. REFERENCES

1. Aluminum-Lithium Alloys, Vols. I, II and III, T.H. Sanders, Jr., and E.A. Starke, Jr., eds., MCEP Ltd., Birmingham, UK (1989).

2. Aluminum Alloys - Physical and Mechanical Properties Vols. I and II, E.A. Starke, Jr. and T.H. Sanders, Jr., eds., EMAS Ltd., Warley, West Midlands, UK (1986).

3. Aluminum-Lithium Alloys III, C. Barker, P.J. Gregson, S.J. Harris and C.J. Peel, eds., Institute of Metals, Oxford, UK, (1986).

4. Aluminum-Lithium Alloys II, T.H. Sanders, Jr., and E.A. Starke, Jr., eds., TMS-AIME, Warrendale, PA (1984).

5. Aluminum-Lithium Alloys, T.H. Sanders, Jr. and E.A. Starke, Jr., eds., TMS-AIME, Warrendale, PA (1981).

6. K.T. Venkateswara Rao, W. Yu and R.O. Ritchie, Metall. Trans. A, Vol. 20A, pp. 485-497 (1989).

7. J. Glazer, S.L. Verzasconi, R.R. Sawtell and J.W. Morris, Metall. Trans. A, Vol. 18A, pp. 1695-1701 (1987).

8. S. Suresh, A.K. Vasudevan, M. Tosten and P.R. Howell, Acta Metall., Vol. 35, pp. 25-46 (1987).

9. R.C. Dorward, Scripta Met., Vol. 20, pp. 1379-1383 (1986).

10. R.G. Buchheit, J.P. Moran and G.E. Stoner, Corrosion, Vol. 46, pp. 610-617 (1990).

11. C. Kumai, J. Kusinski, G. Thomas and T.M. Devine, Corrosion, Vol. 45, pp. 294-302 (1989).

12. E.L. Colvin, G.L. Cahen, Jr., G.E. Stoner and E.A. Starke, Jr., Corrosion, Vol. 42, pp. 416-421 (1986).

13. P. Niskanen, T.H. Sanders, Jr., J.G. Rinker and M. Marek, Corrosion Science, Vol. 22, pp. 283-304 (1982).

14. J.G. Craig, R.C. Newman, M.R. Jarrett and N.J.H. Holroyd, J. De Physique, Colloque C3, Supplement 9, Paper 48, pp. 825-833 (1987).

15. J.B. Lumsden and A.T. Allen, Corrosion, Vol. 44, pp. 527-532 (1988).

16. R.C. Dorward and K.R. Hasse, Corrosion, Vol. 44, No. 12, pp. 932-941 (1988).

17. A.K. Vasudevan, P.E. Bretz, A.C. Miller and S. Suresh, Matls. Sci. Engr., Vol. 64, pp. 113-122 (1984).

18. K.T. Venkateswara Rao, R.S. Piascik, R.P. Gangloff and R.O. Ritchie, Aluminum-Lithium Alloys, T.H. Sanders, Jr. and E.A. Starke, Jr., eds., Materials and Component Engineering Publications Ltd., Birmingham, UK, pp. 955-971 (1989).

19. K. Jata and E.A. Starke, Jr., Metall. Trans A, Vol. 17A, pp. 1011-1026 (1986).

20. K.T. Venkateswara Rao, W. Yu and R.O. Ritchie, Metall. Trans. A, Vol. 19A, pp. 549-561 (1988).

21. K.T. Venkateswara Rao, W. Yu and R.O. Ritchie, Metall. Trans. A, Vol. 19A, pp. 563-569 (1988).

22. N.J.H. Holroyd, in Environment Induced Cracking of Metals, R.P. Gangloff and M.B. Ives, eds., NACE, Houston, TX, pp. 311-346 (1990).

23. R.P. Gangloff, in Environment Induced Cracking of Metals, R.P. Gangloff and M.B. Ives, eds., NACE, Houston, TX, pp. 55-109 (1990).

24. J.A. Feeney, J.C. McMillan and R.P. Wei, Met. Trans., Vol. 1, pp. 1741-1757 (1970).

25. T.H. Shih and R.P. Wei, Engr. Fract. Mech., Vol. 18, pp. 827-837 (1983).

26. J.C. Radon, Metal Science, pp. 411-419, July (1979).

27. M. Gao, P.S. Pao and R.P. Wei, Metall. Trans. A, Vol. 19A, pp. 1739-1750 (1988).

28. R.P. Wei, P.S. Pao, R.G. Hart, T.W. Weir and G.W. Simmons, Metall. Trans. A, Vol. 11A, pp. 151-158 (1980).

29. J. Petit and A. Zeghloul, in Environmentally Assisted Cracking: Science and Engineering, ASTM-STP 1049, W.B. Lisagor, T.W. Crooker, and B.N. Leis, eds., ASTM, Philadelphia, PA, pp. 334-346 (1989).

30. F.J. Bradshaw and C. Wheeler, Intl. J. Fract. Mech., Vol. 5, pp. 255-268 (1969).

31. R.E. Stoltz and R.M. Pelloux, Metall. Trans., Vol. 3, pp. 2433-2441 (1972).

32. H.J.H. Holroyd and D. Hardie, Corrosion Science, Vol. 23, No. 6, pp. 527-546 (1983).

33. M.O. Speidel, M.J. Blackburn, T.R. Beck and J.A. Feeney, in Corrosion Fatigue, Chemistry, Mechanics and Microstructure, O. Devereux, A.J. McEvily and R.W. Staehle, eds., NACE, Houston, TX, pp. 324-345 (1972).

34. A.M. Green and J.F. Knott, in Advances in Fracture Research, K. Salama, K. Ravi-Chandar, D.M.R. Taplin and P. Rama Rao, eds., Pergamon Press, NY, pp. 1747-1756 (1989).

35. F.S. Lin and E.A. Starke, Jr., in Hydrogen Effects in Metals, I.M. Bernstein and A.W. Thompson, eds., TMS-AIME, Warrendale, PA, pp. 485-492 (1981).

36. F.S. Lin and E.A. Starke, Jr., Matls. Sci. and Engr., Vol. 43, pp. 65-76 (1980).

37. R.E. Ricker and D.J. Duquette, Metall. Trans. A, Vol. 19A, pp. 1775-1783 (1988).

38. A. Niegel, H.-J. Gudladt and V. Gerold, in Fatigue '87, R.O. Ritchie and E.A. Starke, Jr., eds., EMAS, West Midlands, UK, pp. 1229-1238 (1987).

39. A. Niegel, H.-J. Gudladt and V. Gerold, J. de Physique, Colloque C5, Vol. 49, pp. 659-663 (1988).

40. R.P. Wei and R.P. Gangloff, in Fracture Mechanics: Perspectives and Directions, ASTM STP 1020, R.P. Wei and R.P. Gangloff, eds., ASTM, Philadelphia, Pa, pp. 233-264 (1989).

41. F.P. Ford, Corrosion, Vol. 35, pp. 281-287 (1979).

42. N.M. Grinberg, Intl. J. Frac., April, pp. 83-95 (1982).

43. Fatigue Crack Growth Threshold Concepts, D. Davidson and S. Suresh, eds., TMS-AIME, Warrendale, PA, pp. 25-42 (1984).

44. R.P. Gangloff and R.O. Ritchie, Fundamentals of Deformation and Fracture, B.A. Bilby, K.J. Miller and J.R. Willis, eds., Cambridge University Press, Cambridge, UK, pp. 529-558 (1985).

45. N.J.H. Holroyd, A.K. Vasudevan and L. Christodoulou, in Treatise on Matls. Sci. and Tech., Vol. 31, A.K. Vasudevan and R.D. Doherty, eds., Academic Press, Boston, MA, pp. 463-483 (1989).

46. J.P. Moran, "Mechanisms of Localized Corrosion and Stress Corrosion Cracking of an Al-Li-Cu Alloy", PhD. Dissertation, University of Virginia, Charlottesville, VA (1990).

47. G.R. Yoder, P.S. Pao, M.A. Imam and L.A. Cooley, in Aluminum-Lithium Alloys, T.H. Sanders, Jr. and E.A. Starke, Jr., eds., MCEP Ltd., Birmingham, UK, pp. 1033-1037 (1989).

48. P.S. Pao, M.A. Imam, L.A. Cooley and G.R. Yoder, Corrosion, Vol. 45, pp. 530-535 (1989).

49. K.S. Shin and S.S. Kim, "Environmental Effects on Fatigue Crack Propagation of a 2090 Al-Li Alloy", in Effects of Hydrogen on Material Behavior, A.W. Thompson and N.R. Moody, eds., TMS, Warrendale, PA, in press (1990).

50. K.S. Shin and E.W. Lee, in Light Weight Alloys for Aerospace Applications, E.W. Lee, E.H. Chia and N.J. Kim, eds., TMS-AIME, Warrendale, PA, pp. 171-179 (1989).

51. J.K. Donald, Unpublished Research, Fracture Technology Associates, Springtown, PA (1989).

52. W.A. Herman, R.W. Hertzberg and R. Jaccard, Fat. Engr. Matls. and Structures, Vol. 11, pp. 303-320 (1988).

53. R.P. Gangloff, Metall. Trans. A, Vol. 16A, pp. 953-969 (1985).

54. R.S. Piascik, "Mechanisms of Intrinsic Damage Localization During Corrosion Fatigue: Al-Li-Cu System", PhD. Dissertation, University of Virginia, Charlottesville, VA (1990).

55. R.S. Piascik and R.P. Gangloff, in Advances in Fracture Research, K. Salama, K. Ravi-Chandar, D.M.R. Taplin and P. Rama Rao, eds., Pergamon Press, NY, pp. 907-918 (1989).

56. R.S. Piascik and R.P. Gangloff, in Environmental Cracking of Metals, R.P. Gangloff and M.B. Ives, eds., NACE, Houston, TX, pp. 233-240 (1990).

57. R.S. Piascik and R.P. Gangloff, "Environmental Fatigue of An Al-Li-Cu Alloy: Part II- Mechanisms of Intrinsic Damage Localization", to be submitted to Metall. Trans. A (1990).

58. H. Tada, P.C. Paris and G.R. Irwin, The Stress Analysis of Cracks Handbook, Del Research Corp., St. Louis, MO, p. 2-10 (1987).

59. R.O. Ritchie and J. Lankford, in Small Fatigue Cracks, R.O. Ritchie and J. Lankford, eds., TMS-AIME, Warrendale, PA, pp. 1-5 (1986).

60. R.P. Gangloff, in Advances in Crack Length Measurement, C.J. Beevers, ed., EMAS, Ltd., Warley, West Midlands, UK, pp. 175-229 (1982).

61. R.P. Gangloff, D.C. Slavik, R.S. Piascik and R.H. Van Stone, "Direct Current Electrical Potential Measurement of the Growth of Small Fatigue Cracks", in Small Crack Test Methods, ASTM STP, J.M. Larsen and J.E. Allison, eds., ASTM, Philadelphia, PA, in review (1990).

62. R.P. Gangloff, Fat. Engr. Matls. and Structures, Vol. 4, No. 1, pp. 15-33 (1981).

63. J.W. Swanson and H.L. Marcus, Metall. Trans. A, Vol. 6A, pp. 291-293 (1978).

64. R.M.N. Pelloux, Trans. ASM, Vol. 62, pp. 281-285 (1969).

65. D.A. Meyn, Trans. ASM, Vol. 61, pp. 52-61 (1968).

66. R.P. Wei, Intl. J. Frac. Mech., Vol. 4, pp. 159-170 (1968).

67. D.J. Shaw, Introduction to Colloid and Surface Chemistry, Butterworths, Boston, MA (1980).

68. P.S. Pao, Ming Gao and R.P. Wei, in Basic Questions in Fatigue: Vol. II, ASTM 924, W.P. Wei and R.P. Gangloff, eds., ASTM, Philadelphia, PA, pp. 182-195 (1988).

69. D.L. Dicus, in Environment-Sensitive Fracture: Evaluation and Comparison of Test Methods, ASTM STP 821, S.W. Dean, E.N. Pugh and G.M. Ugiansky, eds., ASTM, Philadelphia, PA, pp. 513-533 (1984).

70. Jing Gui and T.M. Devine, Scripta Metall., Vol. 21, pp. 853-857 (1987).

71. R.G. Buchheit, F.D. Wall, G.E. Stoner and J.P. Moran, "SCC of Al-Li-Cu-Zr Alloy 2090 in Aqueous Cl and Mixed CO_3^-/Cl Environments", Paper No. 99, Corrosion 91, NACE, Houston, TX (1991).

72. G.R. Yoder, L.A. Cooley and T.W. Crooker, Scripta Met., Vol. 16, pp. 1021-1025 (1982).

73. G.R. Yoder, L.A. Cooley and T.W. Crooker, in Frac. Mech.: Fourteenth Symposium, ASTM STP 791, Vol. 1, J.C. Lewis and G. Sines, eds., ASTM, Philadelphia, PA, pp. 348-365 (1983).

74. G.R. Yoder, L.A. Cooley and T.W. Crooker, in Titanium 80, Proc. 4th Intl. Conf. on Titanium, Vol. 3, H. Kimura and O. Izumi, eds., AIME, Warrendale, PA, pp. 1865-1874 (1981).

75. R.J.H. Wanhill, in "Short Crack Behavior in an Aluminum Alloy - An AGARD Cooperative Test Program", J.C. Newman, Jr. and P.R. Edwards, eds., AGARD Report No. AGARD-R-732, Annex A (1989).

76. G.G. Garrett and J.F. Knott, Acta Metallurgica, Vol. 23, pp. 841-848 (1975).

77. A.J. McEvily and R.P. Wei, in Corrosion Fatigue: Chemistry, Mechanics and Microstructure, O. Devereux, A.J. McEvily and R.W. Staehle, eds., NACE, Houston, TX, pp. 381-395 (1972).

78. D. Aliaga and E. Budillon, "Corrosion Fatigue Behavior of Some Aluminum Alloys", AGARD Report No. AGARD-CP-616 (1981).

79. R.J. Selines and R.M. Pelloux, Met. Trans., Vol. 3, pp. 2525-2531 (1972).

80. D.L. Davidson and J. Lankford, in Fatigue Mechanisms: Advances in Quantitative Measurement of Physical Damage, ASTM STP 811, J. Lankford, D.L. Davidson, W.L. Morris and R.P. Wei, eds., ASTM, Philadelphia, PA, pp. 371-399 (1983).

81. D.L. Davidson and J. Lankford, Matls. Sci. and Engr., Vol. 74, pp. 189-199 (1985).

82. Atlas of Electrochemical Equilibria in Aqueous Solutions, M. Pourbaix, NACE, Houston, TX, pp. 168-176 (1974).

83. F.D. Bogar and T.W. Crooker, NRL Report 8153, Naval Research Laboratory, Washington, DC (1977).

84. M.O. Speidel, Metall. Trans. A, Vol. 6A, pp. 631-651 (1975).

85. R.P. Wei, Ming Gao and P.S. Pao, Scripta Metall., Vol. 18, pp. 1195-1198 (1984).

86. N.J.H. Holroyd and G.M. Scamans, Scripta Metall., Vol. 19, pp. 915-916 (1985).

Table 1: Chemical Composition (by weight percentage)

Alloy	Li	Cu	Zr	Zn	Mg	Fe	Si	Mn	Cr	Ni	Ti	Na	Ca	H
2090	2.14	2.45	0.09	0.01	a	0.05	0.04	a	a	a	0.01	10[b]	5[b]	8.1[c]
7075	d	1.58	0.01	5.74	2.31	0.26	0.10	0.05	0.20	0.01	0.05	d	1[b]	--

[a] Lower than detection limit of 0.00 wt%.
[b] Parts-per-million by weight (ppm).
[c] Average of three measurements, varying between 6.3 and 10.9 ppm.
[d] Lower than detection limit of 0.000 wt%.

Table 2: Tensile Properties of Peak Aged Alloys (Longitudinal)

Alloy	σ_y(MPa)	σ_u(MPa)	Elongation (%)
2090	496	517	6.0
7075	466	540	11.8
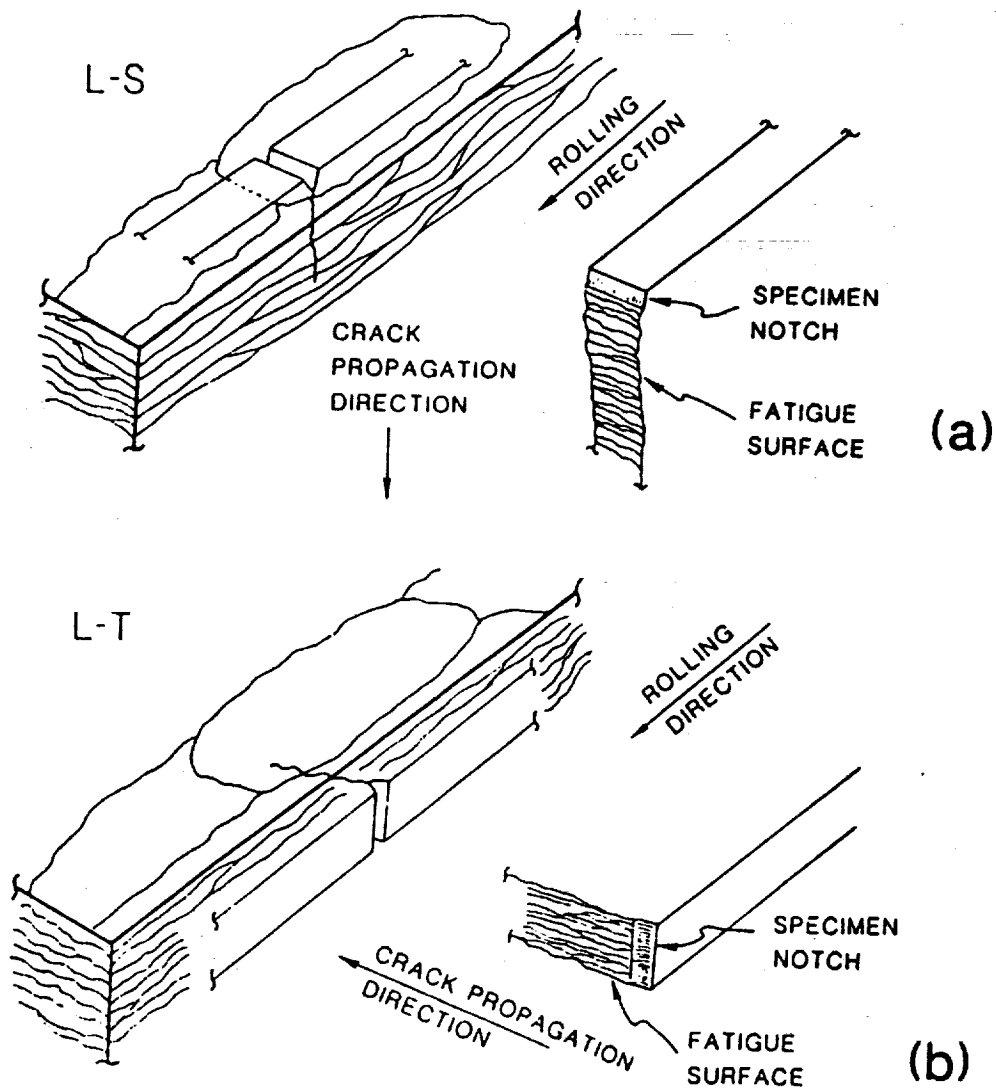
Figure 1   Schematic diagrams of the (a) L-S/single grain and (b) L-T/multiple grain fatigue crack orientations in the microstructure of 2090 rolled plate.
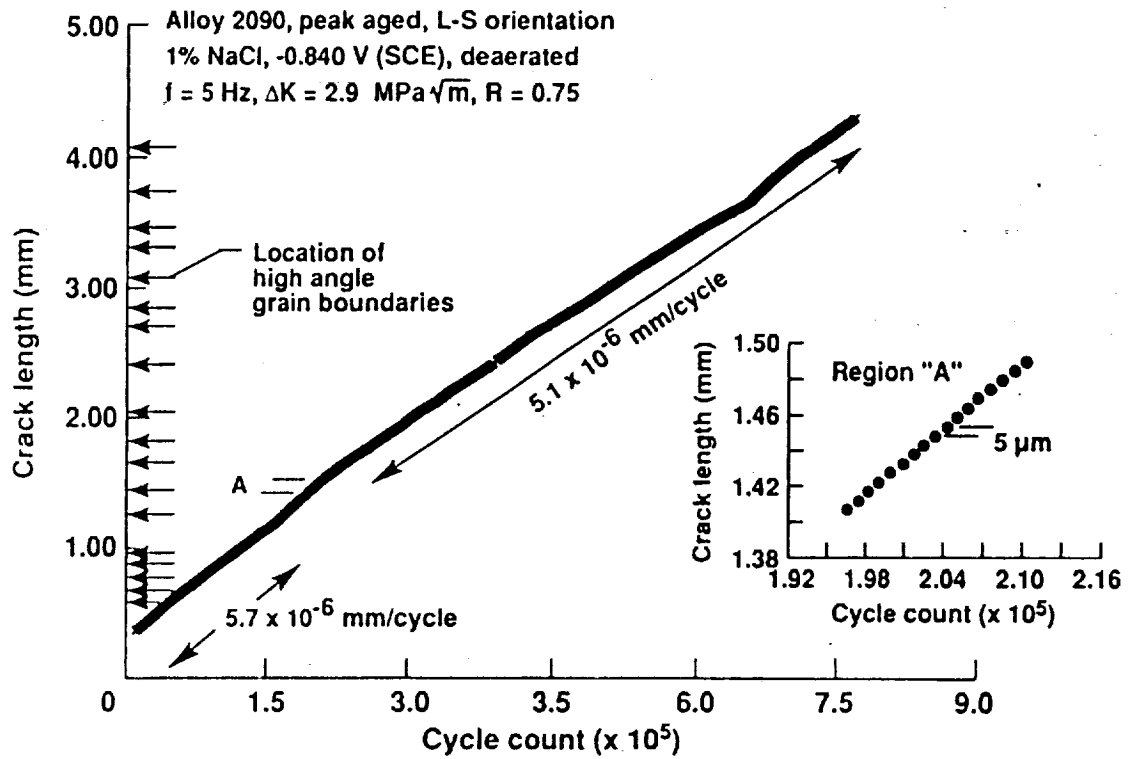
Figure 2 Fatigue crack length versus loading cycles at constant ΔK (2.9 MPa√m, R = 0.75) for peak aged alloy 2090 (L-S/single grain orientation) in 1% NaCl with anodic polarization (-0.840 V). Note the lack of an effect of high angle grain boundaries (arrows) and the 1 μm crack length resolution (insert amplifying Region A).
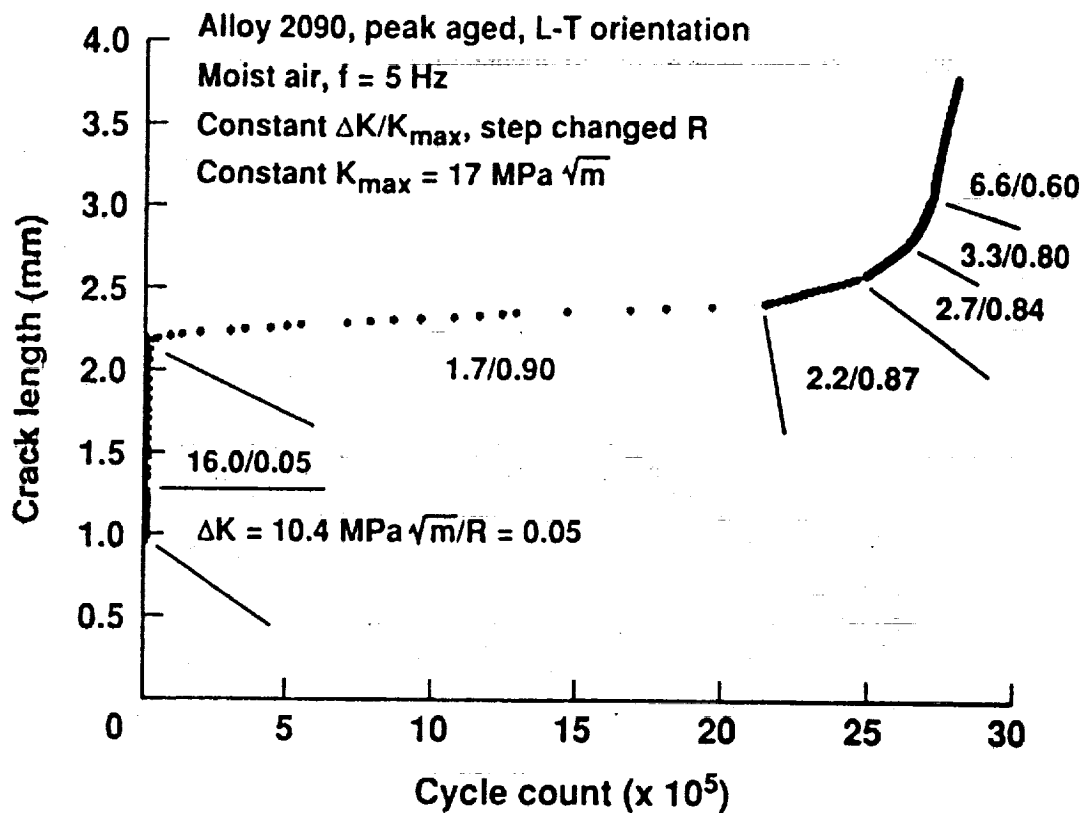
Figure 3 Crack length versus loading cycles plot showing the results of a constant ΔK and K_{max} step changed R test for peak aged alloy 2090 (L-T) in moist air. ΔK and R are noted for each level of constant ΔK at K_{max} = 17 MPa/m. (Exception: K_{max} = 10.9 MPa/m for the first Δa interval.)

Alloy 2090, peak aged
Moist air, f = 5 Hz
$K_{max} = 17$ MPa $\sqrt{m}$

○ L-S orientation
△ L-T orientation
□ L-T, constant ΔK, R = 0.54
◇ L-S, constant ΔK, R = 0.60
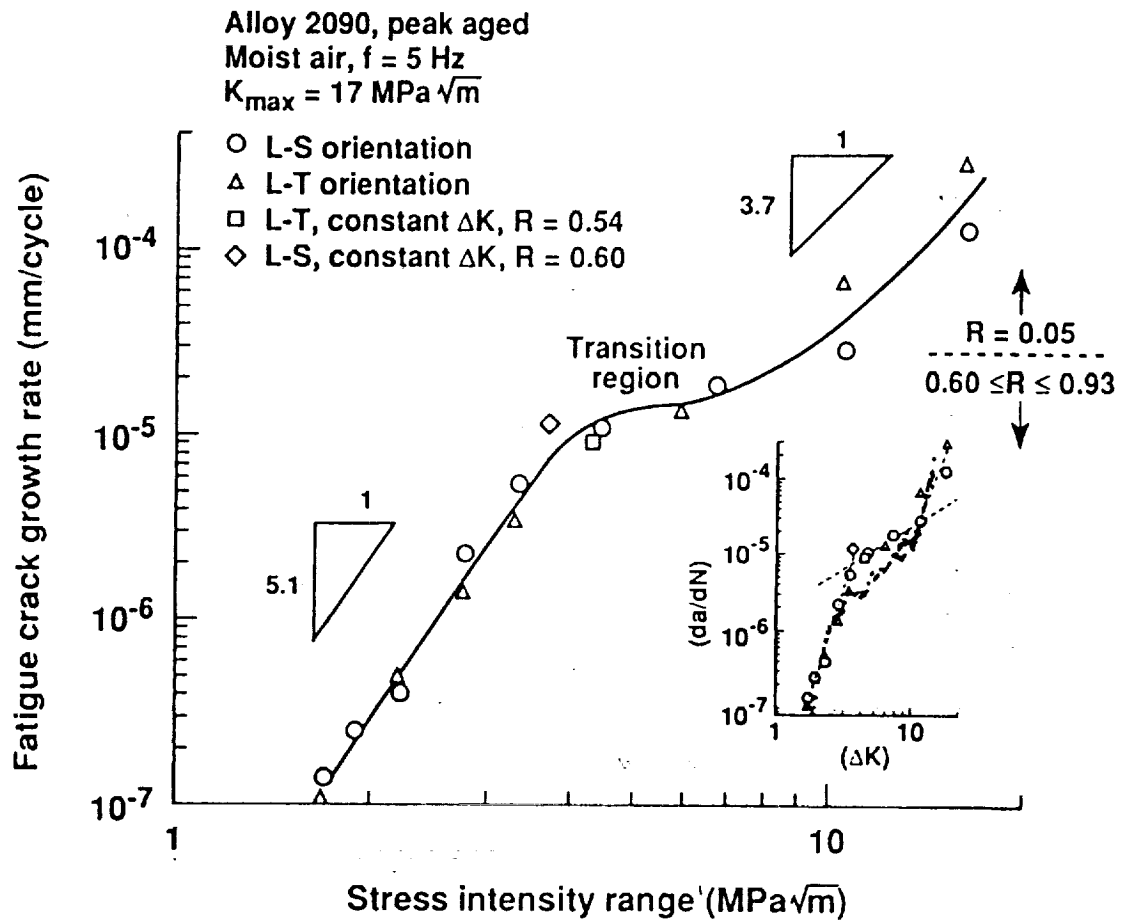
Figure 4   A comparison of intrinsic fatigue crack growth in two orientations of alloy 2090 in moist air for constant K_{max} = 17 MPa/m at 5 Hz. (Exception: K_{max} = 10.9 MPa/m for ΔK = 10.4 MPa/m.) The insert shows the results of a compact tension experiment, based on decreasing ΔK at constant K_{max} (17 MPa/m) for the L-T orientation of 2090[54,55].
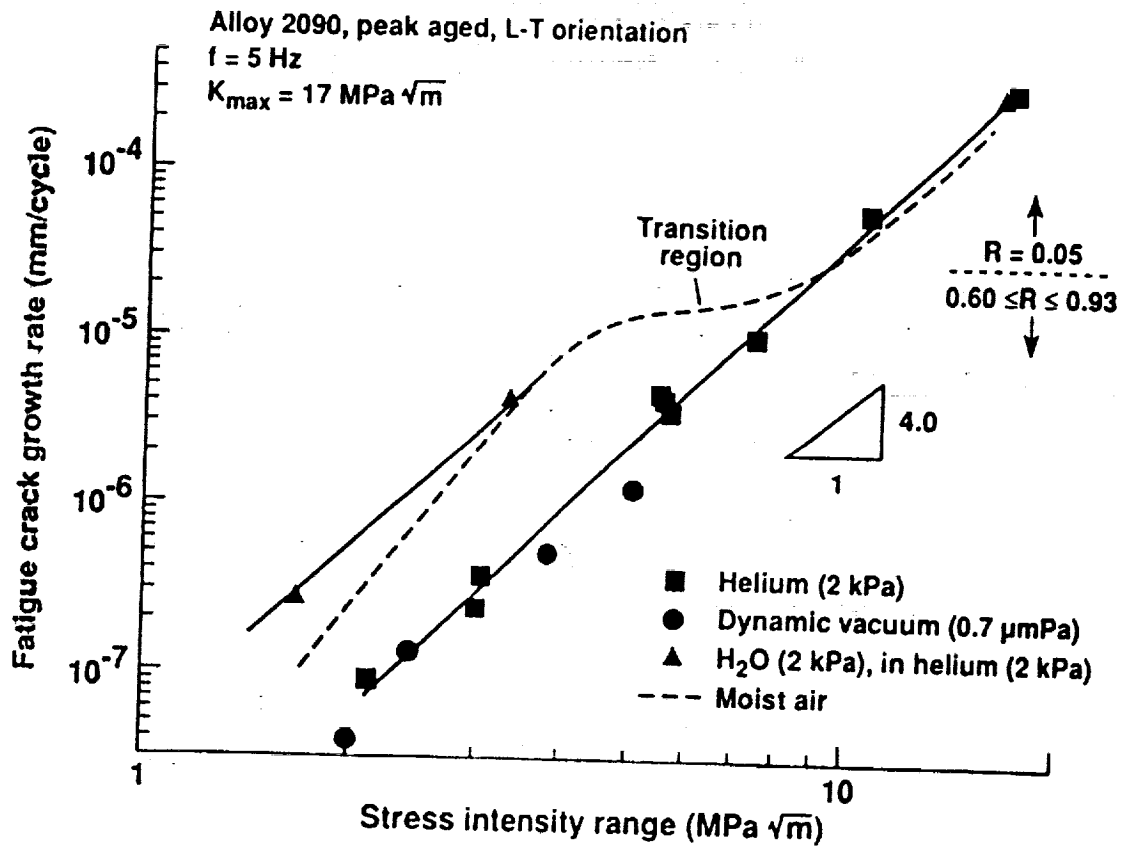
Figure 5 The intrinsic fatigue crack growth behavior of peak aged alloy 2090 (L-T orientation) in vacuum, helium, water vapor and moist air. (Constant K_{max} = 17 MPa/m except for ΔK = 10.4 MPa/m where K_{max} = 10.9 MPa/m; 5 Hz).

Alloy 2090 (L-T) and 7075 (L-S), peak aged
$f = 5$ Hz, $K_{max} = 17$ MPa $\sqrt{m}$

○ 7075 Water vapor (2 kPa)
□ 7075 Helium (2 kPa)
● 7075 Dynamic vacuum (0.7 µPa)
▲ 2090 Dynamic vacuum (0.7 µPa)
■ 2090 Helium (2 kPa)
△ 2090 Water vapor (2 kPa)

$R = 0.05$
$0.60 \leq R \leq 0.93$
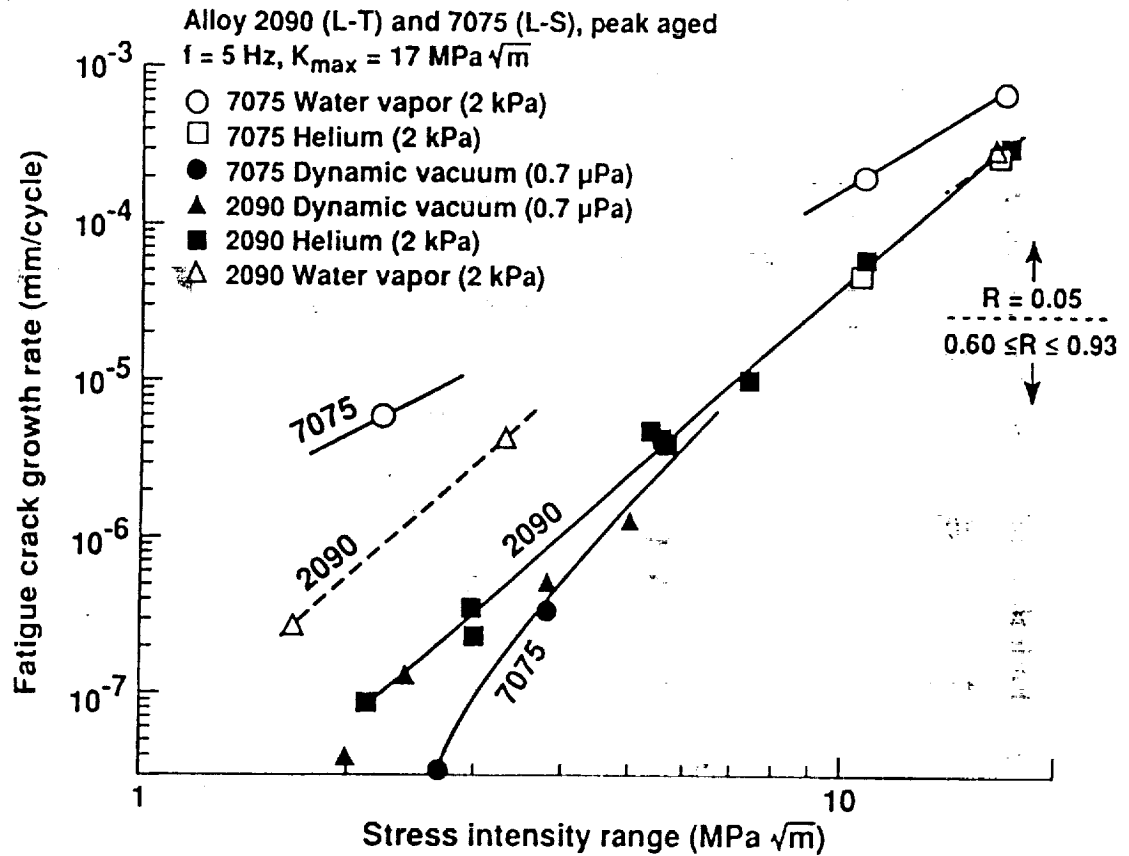
Figure 6   A comparison of the intrinsic corrosion fatigue crack growth behavior of peak aged 2090 (L-T) and 7075-T651 (L-S) at constant K_{max} of 17 MPa/m in water vapor, vacuum and helium; 5 Hz. (Exception: $K_{max} = 10.9$ MPa/m for $\Delta K = 10.4$ MPa/m.)

37
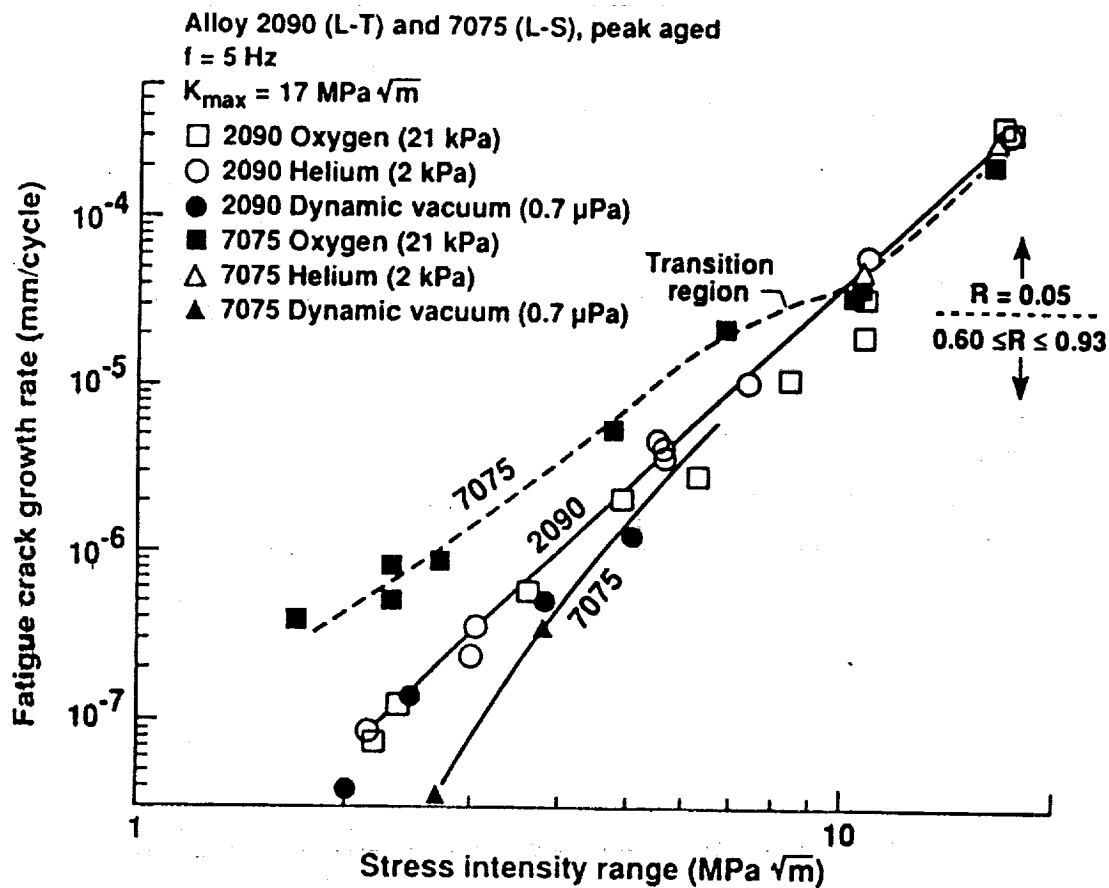
Figure 7   A comparison of the intrinsic fatigue crack growth characteristics of alloys 2090 (L-T) and 7075-T651 (L-S) in purified oxygen, helium and dynamic vacuum. (Constant K_{max} = 17 MPa√m; 5 Hz. Exception: K_{max} = 10.9 MPa√m for ΔK = 10.4 MPa√m.)
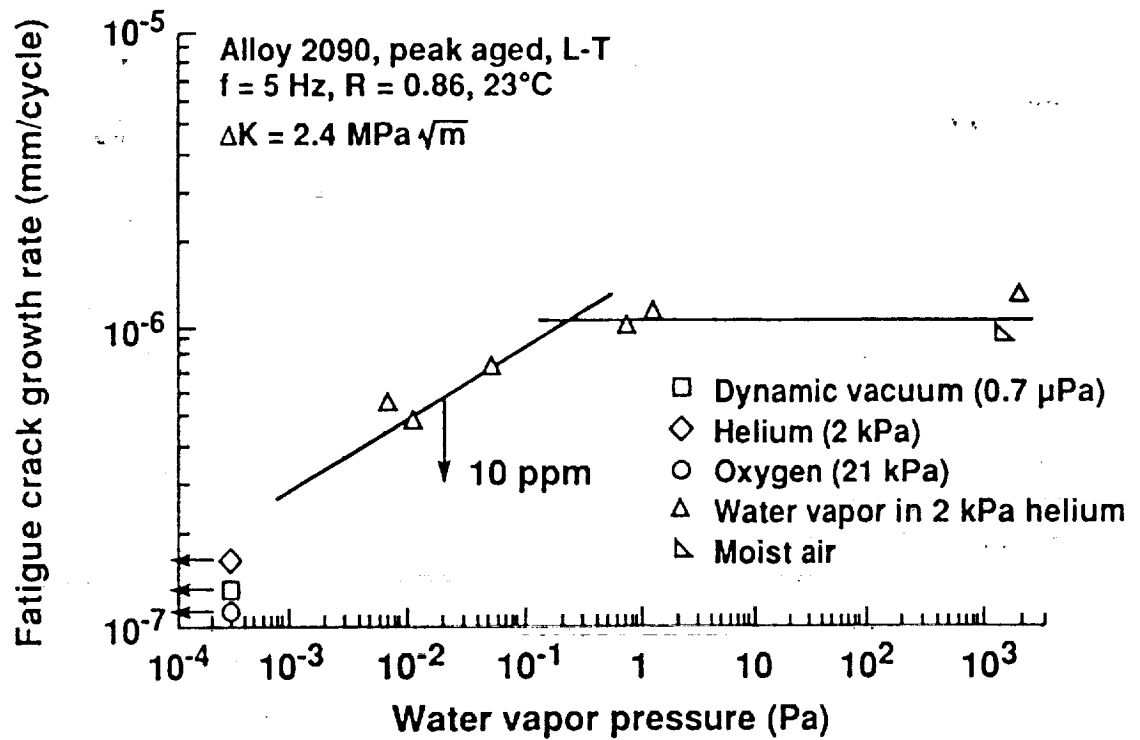
Figure 8   The effect of water vapor pressure on near-ΔK_{th} fatigue crack growth rate in peak aged alloy 2090 (L-T) at constant ΔK (2.4 MPa√m), R (0.86) and frequency (5 Hz).
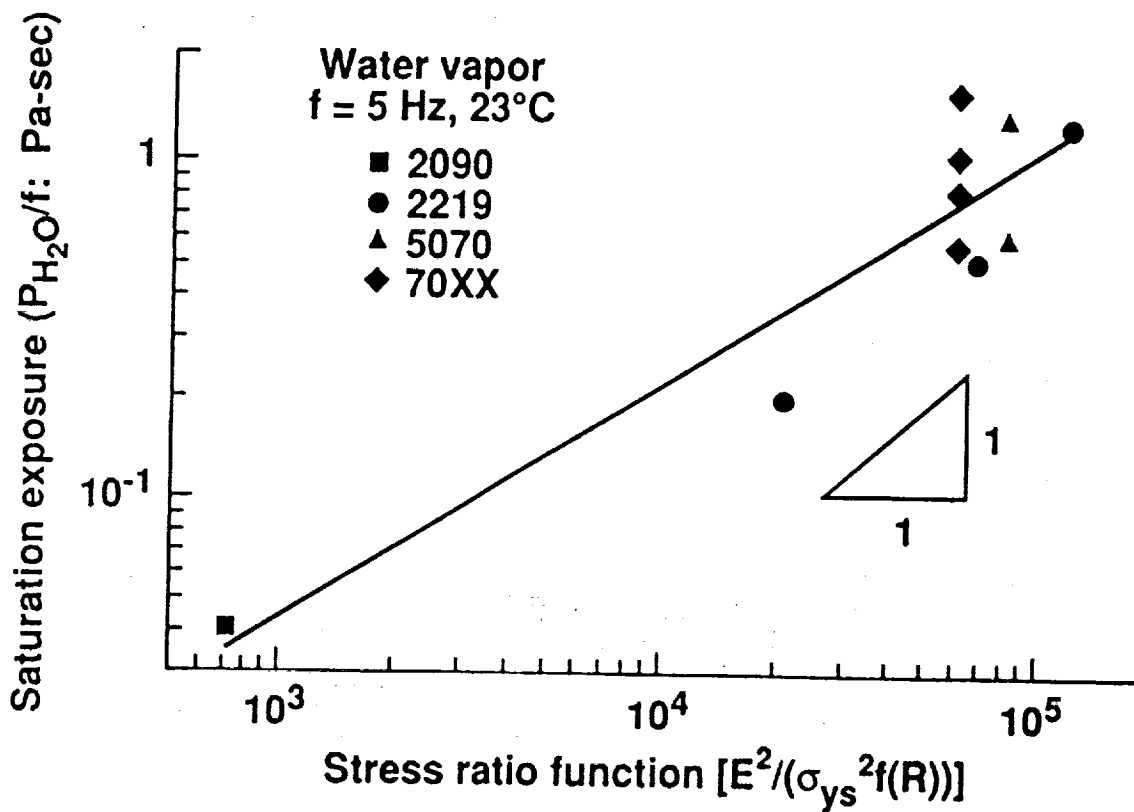
Figure 9 The effect of normalized stress ratio function on the saturation water vapor pressure for exposure-independent da/dN in high strength aluminum alloys, with da/dN rate limited by impeded molecular flow[25,27,28,68,69].
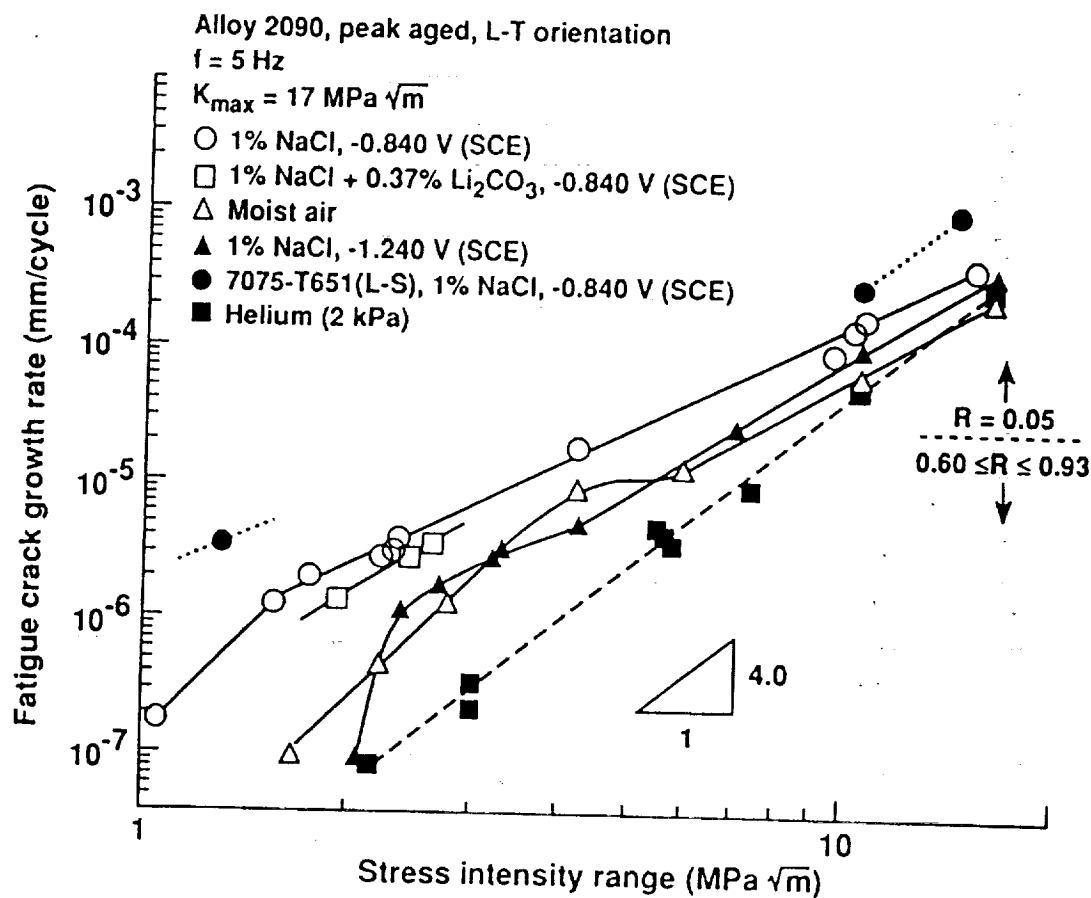
40

Figure 10 Aqueous corrosion fatigue crack growth behavior of peak aged alloy 2090 (L-T) in 1 wt% NaCl at constant anodic (-0.840 V) and cathodic (-1.240 V) potentials, in 1% NaCl + 0.4% Li₂CO₃ (-0.840 V), in moist air and in helium; and of alloy 7075-T651 in aqueous 1% NaCl at constant anodic (-0.840 V) potential. (Constant K_{max} = 17 MPa√m except at ΔK = 10.4 MPa√m where K_{max} = 10.9 MPa√m; 5 Hz).
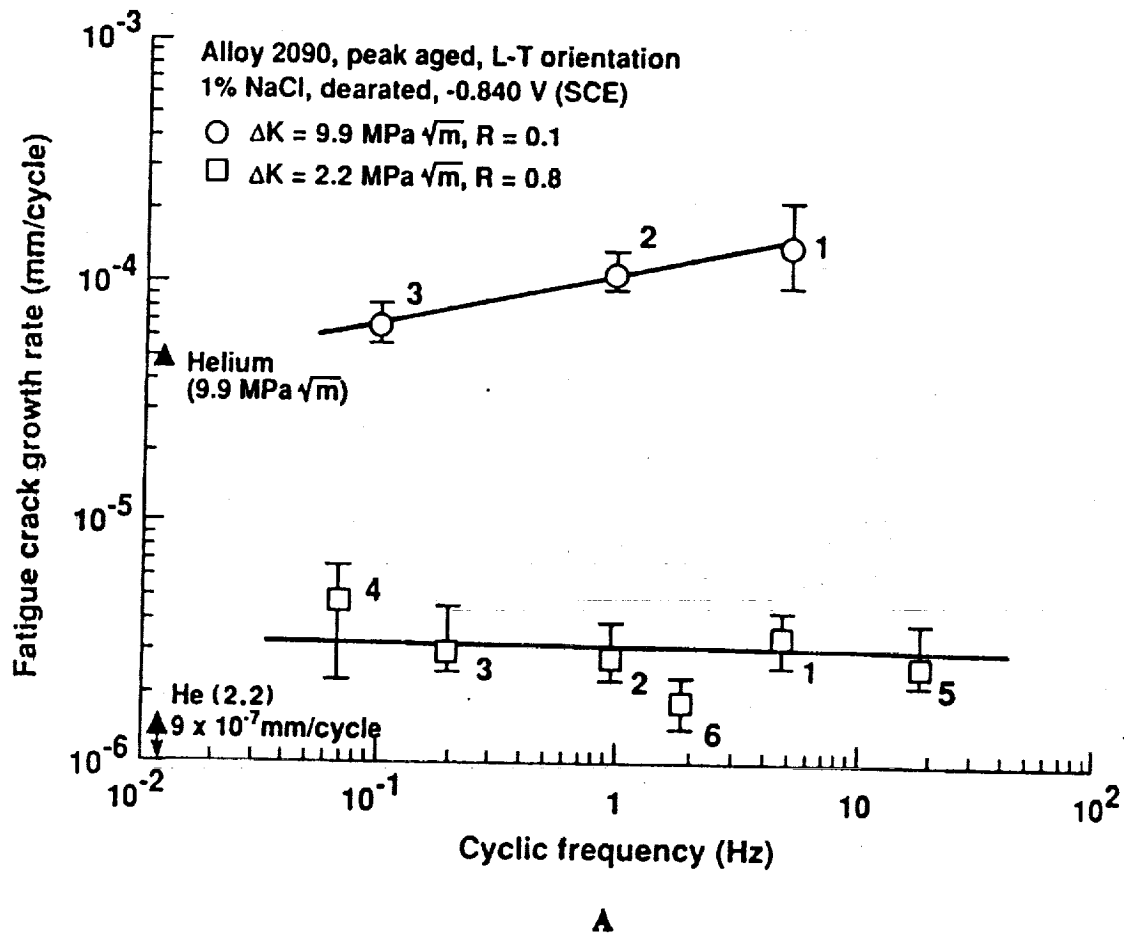
41

Figure 11 The effect of loading frequency on intrinsic FCP rates in peak aged 2090 (L-T) in 1% NaCl (-0.840 V). (a) Da/dN versus f at high and low constant ΔK levels, and (b) crack length versus load cycles at high constant ΔK and loading frequencies of 0.1 Hz, 1 Hz and 5 Hz.
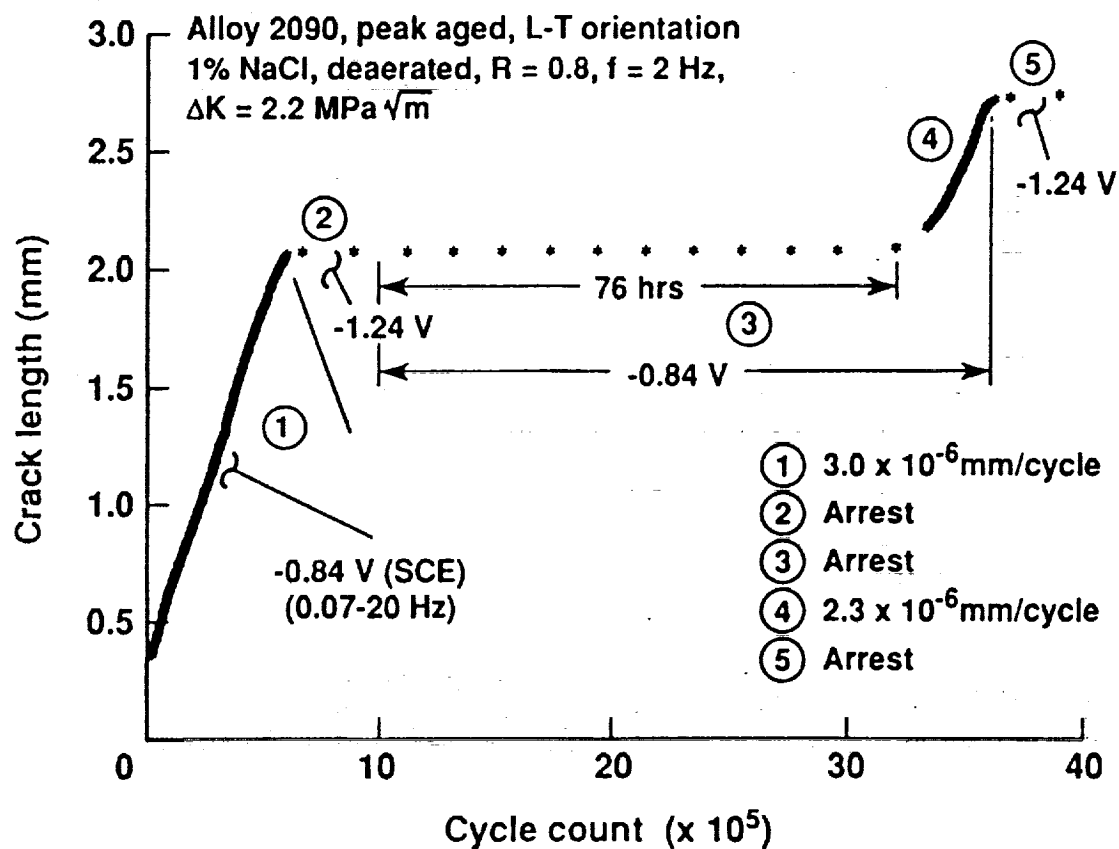
Alloy 2090 peak aged, L-T orientation
$\Delta K = 9.9$ MPa $\sqrt{m}$, R = 0.1
1% NaCl, deaerated, -0.840 V (SCE)

0.1 Hz
6.9×10^{-5} mm/cycle
③

1 Hz
1.1×10^{-4} mm/cycle
②

5 Hz
1.4×10^{-4} mm/cycle
①

B

Figure 11   The effect of loading frequency on intrinsic FCP rates in peak aged 2090 (L-T) in 1% NaCl (-0.840 V). (a) Da/dN versus f at high and low constant ΔK levels, and (b) crack length versus load cycles at high constant ΔK and loading frequencies of 0.1 Hz, 1 Hz and 5 Hz.

43
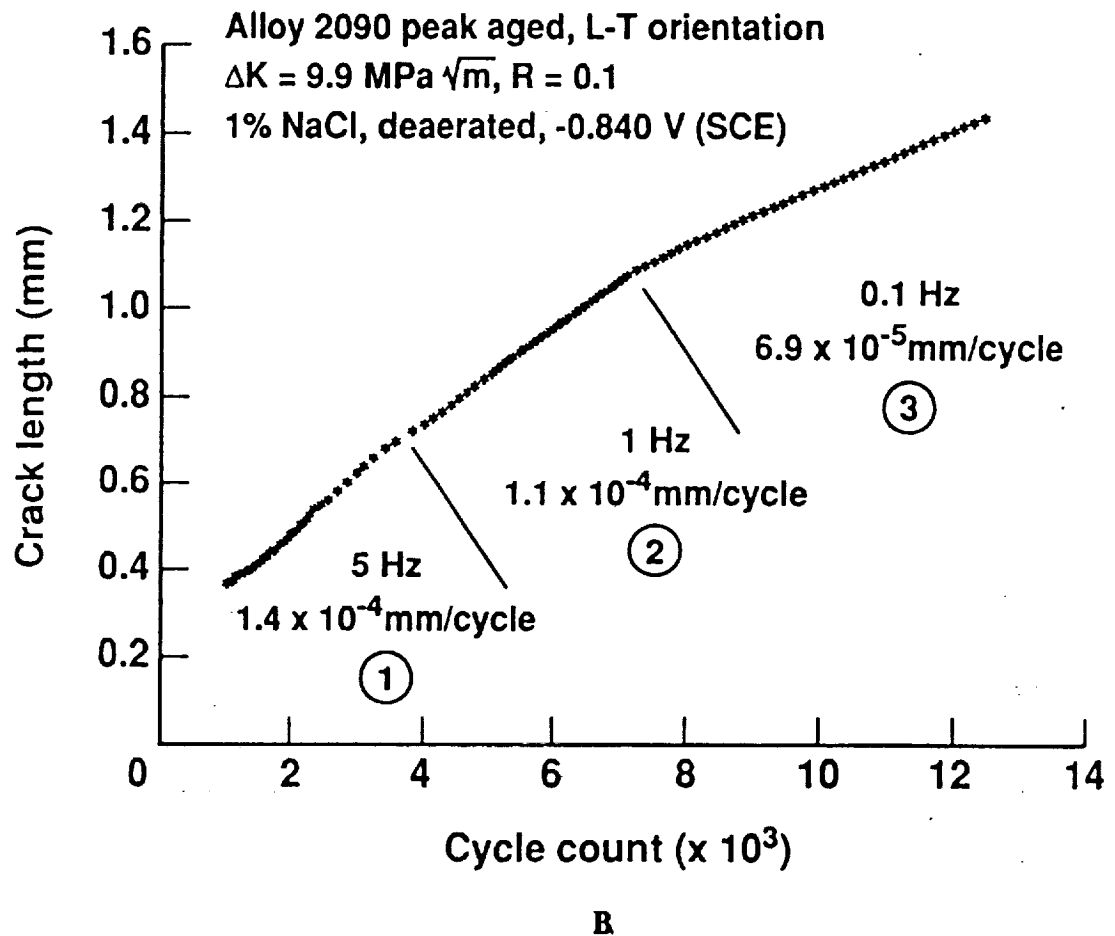
Figure 12 The effect of cathodic polarization on fatigue crack propagation in peak aged 2090 (L-T) in 1% NaCl at a constant ΔK of 2.2 MPa√m and high R.

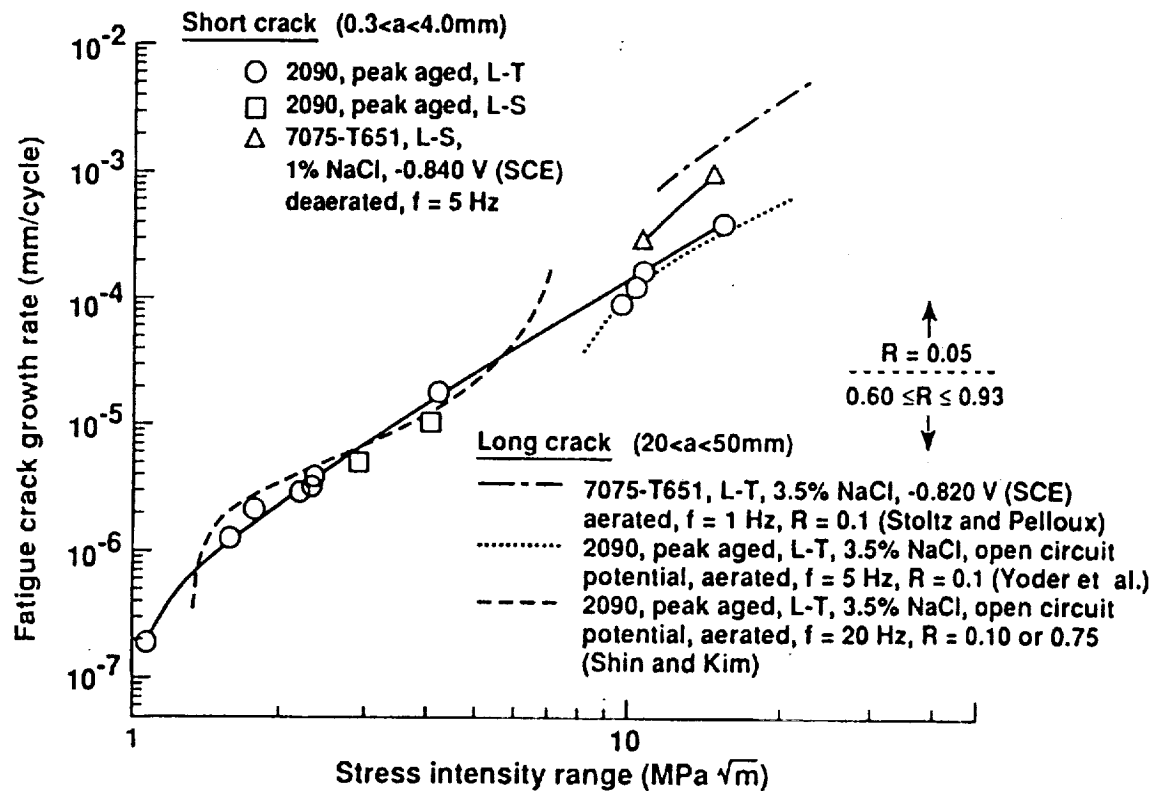*Figure 13* A comparison of the corrosion fatigue crack growth behavior of short cracks (0.3 mm to 4 mm) and long cracks (> 5 mm) for alloys 2090 and 7075 in aqueous NaCl[47-50].

Report Documentation Page

1. Report No.	2. Government Accession No.	3. Recipient's Catalog No.
NASA TM-104064		

4. Title and Subtitle	5. Report Date
Environmental Fatigue of an Al-Li-Cu Alloy: Part I - Intrinsic Crack Propagation Kinetics in Hydrogenous Environments	March 1991
	6. Performing Organization Code

7. Author(s)	8. Performing Organization Report No.
Robert S. Piascik* and Richard P. Gangloff**	

	10. Work Unit No.
9. Performing Organization Name and Address	505-63-01-05
National Aeronautics and Space Administration Langley Research Center Hampton, VA 23665-5225	11. Contract or Grant No.
	13. Type of Report and Period Covered
12. Sponsoring Agency Name and Address	Technical Memorandum
National Aeronautics and Space Administration Washington, DC 20546-0001	14. Sponsoring Agency Code

16. Abstract

Deleterious environmental effects on steady-state, intrinsic fatigue crack propagation (FCP) rates (da/dN) in peak aged Al-Li-Cu alloy 2090 are established by electrical potential monitoring of short cracks with pro-grammed constant ΔK and K_{max} loading. Da/dN are equally unaffected by vacuum, purified helium and oxygen but are accelerated in order of decreasing effectiveness by aqueous 1 percent NaC1 with anodic polarization, pure water vapor, moist air and NaC1 with cathodic polarization. While da/dN depends on $\Delta K^{4.0}$ for the inert gases, water vapor and chloride induce multiple power-laws and a transition growth rate "plateau." Environmental effects are strongest at low ΔK. Crack tip damage is ascribed to hydrogen embrittlement because of: accelerated da/dN due to part-per-million levels of H_2O without condensation, impeded molecular flow model predictions of the measured water vapor pressure dependence of da/dN as affected by mean crack opening, the lack of an effect of film-forming O_2, the likelihood for crack tip hydrogen production in NaC1, and the environmental and ΔK-process zone volume dependencies of the microscopic cracking modes. For NaC1, growth rates decrease with decreasing loading frequency, with the addition of passivating Li_2CO_3 and upon cathodic polarization. These variables increase crack sur-face film stability to reduce hydrogen entry efficiency. The hydrogen environmental FCP resistance of 2090 is similar to other 2000 series alloys and is better than 7075.

17. Key Words (Suggested by Author(s))	18. Distribution Statement
Environmental fatigue Aluminum lithium alloys Fatigue crack propagation Corrosion fatigue	Unclassified - Unlimited Subject Category - 39

19. Security Classif. (of this report)	20. Security Classif. (of this page)	21. No. of pages	22. Price
Unclassified	Unclassified	46	A03